# Exploring the Relative Contribution of the MJO and ENSO to Midlatitude Subseasonal Predictability

Kirsten J Mayer[1], William E Chapman[1], and William A Manriquez[2]

[1]U.S. National Science Foundation National Center for Atmospheric Research
[2]Metropolitan State University of Denver

April 16, 2024

## Abstract

Here we explore the relative contribution of the Madden-Julian Oscillation (MJO) and El Niño Southern Oscillation (ENSO) to midlatitude subseasonal predictive skill of upper atmospheric circulation over the North Pacific, using an inherently interpretable neural network applied to pre-industrial control runs of the Community Earth System Model version 2. We find that this interpretable network generally favors the state of ENSO, rather than the MJO, to make correct predictions on a range of subseasonal lead times and predictand averaging windows. Moreover, the predictability of positive circulation anomalies over the North Pacific is comparatively lower than that of their negative counterparts, especially evident when the ENSO state is important. However, when ENSO is in a neutral state, our findings indicate that the MJO provides some predictive information, particularly for positive anomalies. We identify three distinct evolutions of these MJO states, offering fresh insights into opportune forecasting windows for MJO teleconnections.

# Exploring the Relative Contribution of the MJO and ENSO to Midlatitude Subseasonal Predictability

**Kirsten J. Mayer[1*], William E. Chapman[1*], William A. Manriquez[2]**

[1]U.S. National Science Foundation National Center for Atmospheric Research
[2]Metropolitan State University of Denver
[*]These authors contributed equally

**Key Points:**

- An interpretable neural network is used to decompose contributions of MJO and ENSO to North Pacific subseasonal circulation predictability.
- ENSO alone is overall more useful than the MJO for subseasonal predictions across various lead times and predictand averaging windows.
- Unique MJO events, that provide enhanced subseasonal predictability during ENSO neutral conditions, are identified.

Corresponding authors: Kirsten J. Mayer; William E. Chapman, `kjmayer@ucar.edu`; `wchapman@ucar.edu`

## Abstract

Here we explore the relative contribution of the Madden-Julian Oscillation (MJO) and El Niño Southern Oscillation (ENSO) to midlatitude subseasonal predictive skill of upper atmospheric circulation over the North Pacific, using an inherently interpretable neural network applied to pre-industrial control runs of the Community Earth System Model version 2. We find that this interpretable network generally favors the state of ENSO, rather than the MJO, to make correct predictions on a range of subseasonal lead times and predictand averaging windows. Moreover, the predictability of positive circulation anomalies over the North Pacific is comparatively lower than that of their negative counterparts, especially evident when the ENSO state is important. However, when ENSO is in a neutral state, our findings indicate that the MJO provides some predictive information, particularly for positive anomalies. We identify three distinct evolutions of these MJO states, offering fresh insights into opportune forecasting windows for MJO teleconnections.



## Plain Language Summary

Weather is hard to predict with longer forecast leads. Here, we use a data-driven statistical model to dissect tropical sources of predictability on 2 week to 2 month midlatitude upper-level variability. This model was constructed so that we can identify the relative contributions of two tropical phenomena important for predictability on these timescales. Namely, we use the Madden-Jullian Oscillation (MJO) and the El Niño Southern Oscillation (ENSO) as predictor variables, two phenomena that provide a teleconnecting signal from the tropics to midlatitude variability. We find that the ENSO signal alone consistently provides more forecast predictability than the MJO. However, when ENSO is not active, the MJO provides distinct windows of forecast opportunity, particularly for anomalously anticyclonic events. We identify three evolutions of the MJO which offer new insights into forecasting weather at long forecast leads.


## 1 Introduction

Forecasting for the subseasonal timescale (often defined as 2 weeks through 2 months) has received considerable attention over the last decade (White et al., 2017; Mariotti et al., 2020; Merryfield et al., 2020; White et al., 2021). These timescales are particularly difficult to predict as generally neither atmospheric initial conditions nor slower varying boundary conditions provide sufficient information to make useful predictions (Vitart et al., 2012, 2017; Mariotti et al., 2020). Unfortunately, this is also a timescale in which many public and private sectors seek information to make informed, actionable decisions in order to save lives and property (White et al., 2017, 2021). One way to garner skill on these timescales is to harness predictive skill from specific modes of variability known to provide enhanced subseasonal predictability when the mode is active – termed forecasts of opportunity (Mariotti et al., 2020). One such mode of variability that has gathered considerable attention in the subseasonal community is the Madden-Julian Oscillation (MJO; Madden & Julian, 1971, 1972, 1994).

The MJO consists of two oppositely signed zonally oriented convective anomalies that propagate from the Indian Ocean to the central Pacific, completing a cycle every 20 to 90 days. The associated upper-level circulation anomalies can interact with the subtropical jet, exciting quasi-stationary Rossby waves (Hoskins & Ambrizzi, 1993), which influence midlatitude circulation anomalies on subseasonal timescales. Following specific phases (i.e. locations) of the MJO, this teleconnection can lead to improved prediction skill on subseasonal timescales (Tseng et al., 2018). The MJO teleconnection has been shown to manifest as a Pacific North American (PNA) - like system. In its positive phase, the PNA is characterized by a deepened Aleutian Low, and increased Canadian High, and a deepened Florida low pattern which extends into the Atlantic (Wallace & Gutzler, 1981). The Aleutian Low limb of the PNA, in particular, is responsible for greater downstream effects of precipitation and temperature anomalies across the whole of North America. In observations, the growth of the PNA anomaly is dominated by barotropic energy conversion from the zonally asymmetric climatological flow in the North Pacific storm track (e.g., Feldstein, 2002; Frederiksen, 1983; Simmons et al., 1983). However, a primary mode of Aleutian Low growth is also from excitation by tropical heating, such as from the MJO or El Niño Southern Oscillation (ENSO) Hoskins & Ambrizzi (1993); Sardeshmukh & Hoskins (1988).

ENSO is an interannual coupled ocean-atmosphere mode in the tropical Pacific (Trenberth, 1997), and the primary mode of tropical variability. However, it can also influence the subseasonal timescale through its impact on the MJO (Hendon et al., 1999; Kessler, 2001; Pohl & Matthews, 2007) and the basic state in which MJO teleconnections propagate (Namias, 1986; Moon et al., 2011; Takahashi & Shirooka, 2014), ultimately impacting the MJO's influence in the midlatitudes (Stan et al., 2017; Henderson & Maloney, 2018; Tseng et al., 2020; Arcodia et al., 2020) and subsequent subseasonal prediction skill (Johnson, Collins, Feldstein, L'Heureux, & Riddle, 2014; L. Wang & Robertson, 2019). Further, recent work suggests ENSO may play a main role in changes to midlatitude subseasonal predictability in a future, warmer climate (Mayer & Barnes, 2022). While ENSO is often used for seasonal prediction (e.g., Gibson et al., 2021; Winkler et al., 2001), there is also considerable literature that highlights ENSO teleconnections as a driver of midlatitude subseasonal variability, particularly in boreal winter by also modulating the Aleutian Low (e.g., Kumar & Hoerling, 1998; Chapman et al., 2021). Notably, the ENSO teleconnection exhibits significant evolution throughout a season. This dynamic evolution contributes to heightened predictability and diverse surface responses, contingent on the time of year and the strength of the background flow (the mid-latitude jet). Consequently, this lends support to the suggestion that ENSO could rival the MJO as a dominant driver of subseasonal forecast skill (Chapman et al., 2021).

These results raise the question as to the relative role of the MJO and ENSO in midlatitude subseasonal predictability. Johnson, Collins, Feldstein, L'Heureux, & Riddle (2014) showed that skillfull subseasonal forecasts can be derived solely using the state of the MJO and ENSO. However, given the time-scale of these two modes of variability, the utility of the MJO for midlatitude predictability dwindles as a function of leadtime while the ENSO utility remains a reliable source of longer range predictability. This study seeks to further elucidate the relative roles of both ENSO and MJO for midlatitude subseasonal forecasting using a more complex and interpretable statistical technique. We explore a range of forecast lead times and predictand averaging window lengths to investigate the relative role of these tropical drivers of subseasonal predictability for a variety of forecast criteria.

In recent years, neural networks have been shown to be a powerful statistical tool for the atmospheric sciences due to their ability to identify non-linear, physical relationships within large amounts of data (Toms et al., 2020, 2021; Labe & Barnes, 2022; Martin et al., 2022; Davenport & Diffenbaugh, 2021; Gordon et al., 2021). For example, on subseasonal timescales, explainable neural networks were demonstrated to identify subseasonal forecasts of opportunity using the network's "confidence" in a given prediction as well as the associated tropical sources of predictability through explainability techniques (Mayer & Barnes, 2021). Here we utilize network confidence and an interpretable neural network architecture known as a Neural Additive Model (Agarwal et al., 2020; Gordon et al., 2023), to disentangle the relative contributions of the MJO and ENSO to subseasonal predictability over the North Pacific in the pre-industrial control simulations from the Community Earth System Model. Specifically, we create two artificial neural networks, one of which receives an MJO index while the other receives an ENSO index. The predictions from these two networks are linearly combined to generate the final prediction for the sign of Z500 anomaly over the North Pacific on subseasonal timescales. This allows for the decomposition of a network's prediction into the respective contributions from ENSO and MJO. We find that information about the state of ENSO alone is overall more important than that of the MJO for subseasonal predictability of North Pacific circulation in the pre-industrial simulations. However, the state of the MJO still provides important information particularly for shorter lead time predictions of positive Z500 anomalies during network-identified forecasts of opportunity.

# 2 Data & Methods

## 2.1 Data

We leverage the Community Earth System Model version 2 (CESM2) pre-industrial control run (CESM2-PI) from model years 100-400 from the CMIP6 experiment suite (Danabasoglu et al., 2020). CESM2-PI has interactive land, coupled ocean with biogeochemistry, interacting sea-ice and non-evolving land ice, and constant 1850's CO2 forcing. The model's resolution is nominally 1 degree, with 32 vertical levels. A full description of the CESM2-PI runs can be found in Danabasoglu et al. (2020). From those years we select the daily geopotential height at 500 hpa (Z500), sea surface temperature (SST), and zonal wind at 200 hPa and 850 hPa (U200 and U850, respectively). We then separate the data into three independent data sets: training [model years 100-200], validation [model years 201-300], and testing [model years 301-400]. 100 years of training data was found sufficient to have the machine learning models fully converge on optimal solutions, meaning, adding more data did not significantly change resultant learned network weights. There is concensus that the eastern Pacific teleconnections associated with MJO and ENSO peak during the boreal winter (e.g., Philander, 1985; Henderson et al., 2016; Chapman et al., 2021). Therefore, we focus our investigation exclusively on this seasonal period, restricting our model training and analysis to input dates ranging from November 1st to February 28th. Consequently, the forecasts extend until March 30th, with a lead time of 30 days.

The practical relevance of this study relies on an accurate representation of the analyzed modes of variability in CESM2-PI. The primary rationale for scrutinizing predictability within CESM2-PI, rather than relying on observations, is to augment the size of the datasets used for training, testing, and validating the neural networks. CESM2-PI is recognized as a cutting-edge model, particularly in its representation of the MJO and ENSO, along with their associated North Pacific teleconnections. Numerous studies have evaluated the accuracy of this representation (Danabasoglu et al., 2020; J. Wang et al., 2022; Capotondi et al., 2020). To further corroborate the fidelity of these teleconnections, with particular attention to the task presented to the neural network, we present the frequency of anomalous Z500 signs 5-9 days after an active MJO in phases 3/4 and 6/7 in the supplementary material (Fig. S1), and compare that representation to that in ECMWF's version 5 reanalysis product (ERA5, Hersbach et al., 2020). It is clear that the model represents the MJO teleconnection well, capturing the dominate location and sign of the Z500 anomalous for the two active teleconnection phases of the MJO.

Additionally, the same suite of forecast variables was downloaded from ERA5 (1979-2020), to verify that the ML models results are valid on a global reanalysis product. The ERA5 product is regridded to the common CESM2 grid prior to any reanalysis using a bilinear interpolation scheme (Zhuang et al., 2018).

## 2.2 Methods

### *2.2.1 MJO, ENSO, & Aleutian Low Indices*

We follow the methods of Lin et al. (2008) for calculation of the real-time multivariate MJO indices (RMM1 and RMM2) in the CESM2-PI runs. Starting from the unfiltered observed daily averaged data of the OLR and zonal wind at 850-hPa and 200-hPa from model years 100-400, the time-mean, and the first three harmonics of the daily climatology are removed at every grid-point. Next, the time-series is filtered, by removing the grid-point time-mean of the previous 120 days. Removing the previous 120-day average eliminates most of the interannual variability, including the effects of ENSO. A meridional band average is then taken from 15°S to 15°N for the three fields. Each variable is then normalized by its own zonal average of temporal standard deviation, the fields are combined and decomposed and the two leading EOFs are retained. The resulting structures of the EOF modes are very similar to Wheeler & Hendon (2004, not shown).

The ENSO index is computed by employing a rolling 90-day window and a cosine latitude weighted average of the Sea Surface Temperature (SST) anomaly within the conventional Nino3.4 region [5°N-5°S and 170°W-120°W]. The SST anomaly is determined by subtracting a 60-day rolling average centered on each day of the year.

The target of the neural network is the sign of the Aleutian Low index. The Aleutian Low index is a representation the anomalous geopotential height at 500 hPa in the eastern North Pacific and is determined via the following process: Initially, a 60-day rolling average centered climatology is subtracted from the raw geopotential height data, with each center point corresponding the model day of year. Then the anomalous index within the target region [30°N to 60°N and 190°W to 250°W], is computed via a cosine latitude weighted average. Finally, the target averaging window is established by applying a forward rolling mean to the daily index data, using the desired target window length (2-28 days).

Finally, previous studies have indicated that the wintertime evolution of the basic state is non-trivial (Newman & Sardeshmukh, 1998) and thus tropically derived, eastern Pacific, teleconnections [which feed off the barotropic energy conversion provided by the divergence of the background jet] vary greatly (Chapman et al., 2021; Sardeshmukh & Hoskins, 1988). Thus, we also input the day of the year (DOY), which is represented as a linearly increasing value spanning from the first of November to the final day of February, encompassing all input days. The DOY index is subsequently normalized, ensuring it maintains a zero mean and a standard deviation of unity, prior to its incorporation into the neural network.

### *2.2.2 Interpretable Neural Network*

Figure 1 shows a schematic of the interpretable neural network specifically constructed to dissect the relative contributions of the MJO and ENSO to subseasonal predictability over the North Pacific. Following the general architecture laid out in Gordon et al. (2023), two artificial neural networks are combined at the output layer through a linear combination to create the final output prediction. In our applications, both networks are tasked to predict the sign of the 500 hPa geopotential height anomaly averaged over the North Pacific at the target lead. However, the top network (Figure 1a) only receives information about the state of ENSO and its evolution throughout 15 days prior (hereafter referred to as the ENSO-network) while the bottom network only receives the RMM1 and RMM2 index values and their evolution throughout the 15 days prior (Figure 1b; hereafter referred to as the MJO-network). Additionally, each network receives the DOY associated with $t_0$ as input so that it may also learn variability in sources of predictability within the boreal winter season. The final predictions are taken as the linear combination of the outputs of the individual networks, meaning that the network must learn

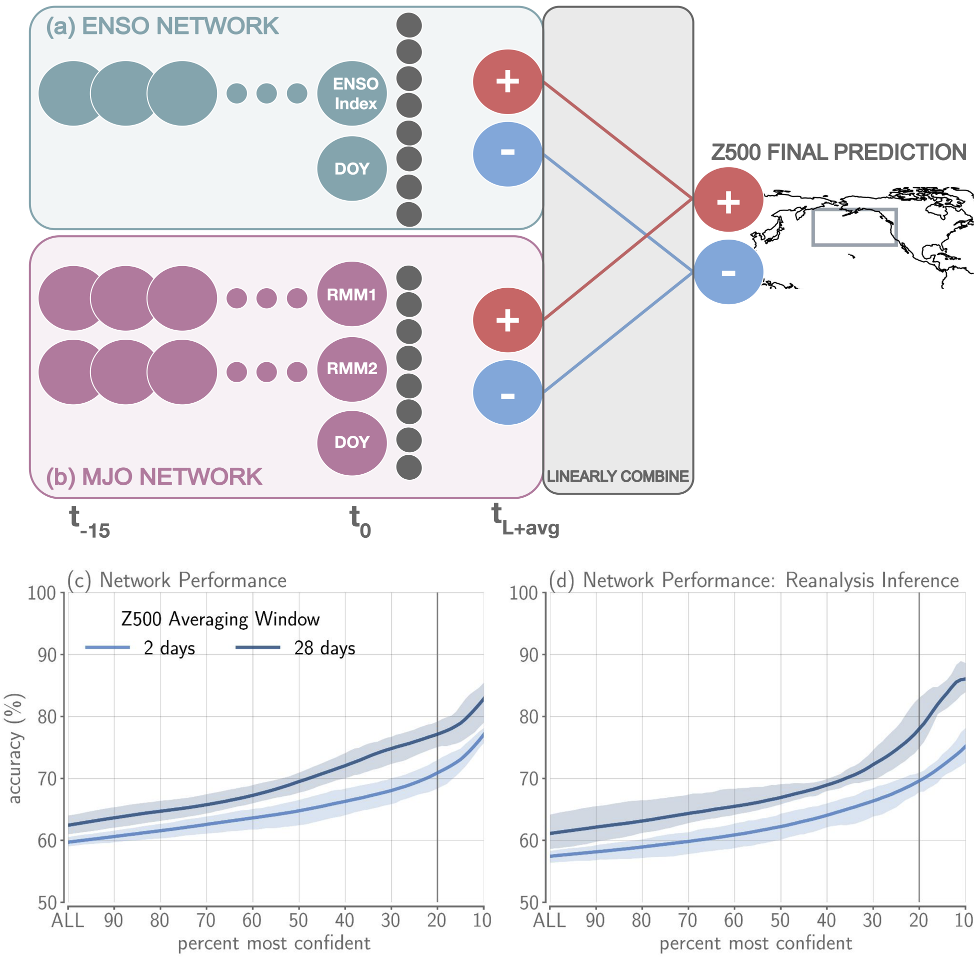


**Figure 1.** Schematic of the interpretable neural network architecture. Input into the (a) ENSO-network includes the ENSO index at $t_0$ plus the 15 days prior ($t_{-15}$) and associated normalized day of year (DOY) at $t_0$ to predict the sign of the Z500 anomaly averaged over North Pacific (grey rectangle) at a specified lead ($t_{L+avg}$, where "L" indicates the lead time and "avg" indicates the Z500 temporal averaging window length). The (b) MJO-network is constructed similarly but instead inputs RMM1 and RMM2 rather than the ENSO index. The predictions from each network are linearly combined (grey shaded box) to make the final network prediction. The bottom two panels include network performance [accuracy] across confidence thresholds for the (c) testing dataset and (d) ERA5 reanalysis. The light/dark blue lines represent the mean accuracy at each confidence level across all lead times (shading) for a Z500 averaging window of 2 days/28 days

to strategically weight its contribution to the final prediction. Therefore, the individual output of each neural network can be considered its contribution to a prediction, allowing interpretation of the specific role of each predictor (i.e., ENSO or MJO) in the network's skill.

To explore the impact of lead and predictand temporal averaging on the source of predictabilty, we train separate neural networks for leads ranging from 5 to 30 days and predictand temporal averaging windows of 2 to 28 days. Furthermore, we train five networks, each with a different random seed per lead and averaging window combination, to assess the network's sensitivity to random initialization weights. Minimal differences between random initializations are observed, leading us to present the results as averages across the five networks.

Both the ENSO- and MJO- networks have one hidden layer with eight nodes and use the rectified linear unit (ReLU) activation function. We note that increasing the complexity of either network does not impact the results [not shown]. To train the model, we use a batch size of 32, categorical crossentropy as the loss function and the Adam Optimizer (Kingma & Ba, 2014) for gradient descent with a learning rate of 0.001. The learning rate is initially held constant for the first 19 epochs and then reduced by 90% after each epoch to help minimize the loss. To reduce overfitting to the training data, training is completed after the validation loss does not improve for 20 epochs, at which time the network weights are reverted to 20 epochs prior. The softmax activation function is applied to the final layer of the total-network (Figure 1) so that the output values sum to one and represent a network estimation of likelihood, or "confidence". Previous research has shown that network confidence can be used to identify forecasts of opportunity when accuracy increases with confidence (Mayer & Barnes, 2021), allowing us to explore the contributions of the MJO and ENSO for all predictions and during network-identified forecasts of opportunity. Here, we define confident predictions as the 20% most confident following (Mayer & Barnes, 2022).

#### *2.2.3 Quantifying Relative Contribution*

We employ two methods to quantify the relative contribution of the ENSO- and MJO- networks to the total-network predictions. The first explores the frequency that the final, total prediction is correctly predicted by a specific network while incorrectly predicted by the other. This illuminates how often either the ENSO- *or* MJO- network solely contributes to the correct total-network prediction while the other network acts incorrectly.

The second metric quantifies the percentage of the total-network accuracy provided by either the ENSO- or MJO- network through permutation importance McGovern et al. (2019). Permutation importance is a technique used to remove relationships between the input and output through randomly shuffling the input data. The subsequent decrease in network performance can then be attributed to the importance of that input data to the prediction. To calculate the importance (percentage of accuracy) contributed by the ENSO-network, we randomly shuffle the ENSO index testing samples (retaining the 15 day memory), calculate the accuracy of the total-network with the randomly shuffled data, and compare it to the accuracy of the total-network without shuffled data. To calculate the percentage of accuracy contributed by the MJO-network, we apply the same technique, but shuffle the RMM indices. We note that the random shuffling does not account for memory between samples, and therefore, the network contribution to the total accuracy could be larger.

# 3 Results

## 3.1 Network Performance

To evaluate network performance, we calculate the accuracy of the network on the testing data across confidence levels (Figure 1c). The testing data is randomly subset to an equal number of positive and negative anomalies so that random chance is 50% for all predictions (N≈11,500; 100% most confident). Across the range of Z500 averaging windows (lines) and lead times (shading), the network performs better than random change at $\geq$ 60% accuracy. We include the two extreme averaging windows (2 and 28 days) for ease of visualization, however, the other averaging windows fall within these two curves. As network confidence increases, the accuracy of the network increases as well, indicating the network is able to identify periods of enhanced predictability (Figure 1c). Further, we find similar performance when the network is evaluated on reanalysis data (Figure 1d), suggesting the network is identifying physically relevant forecasts of opportunity for subseasonal predictability of Z500 anomalies over the North Pacific (Mayer & Barnes, 2021).

Previous work has also detailed the importance of the basic state evolution throughout boreal winter on tropically forced teleconnection propagation and its potential for improved subseasonal predictability (Newman & Sardeshmukh, 1998; Chapman et al., 2021, e.g.). Therefore, to account for any within season evolution of ENSO or MJO teleconnections to North Pacific predictability, DOY is included as an input into the network. We find that when the network is correct (grey histograms in Figure 2), the frequency of predictions are generally consistent across DOY with a slight increase towards the latter end of the season across leads 7 through 28 days. However, when the network is also confident (purple histograms in Figure 2), the frequency of predictions increases at the latter end of boreal winter. We note that the purple histograms become flatter with lead time (i.e. more early winter predictions) since longer lead time predictions made near the beginning of boreal winter are forecasting for the latter part of the season. These results indicate that the network has identified the latter half of boreal winter as a preferable period for enhanced subseasonal predictability, consistent with previous research (Newman & Sardeshmukh, 1998; Chapman et al., 2021). In other words, the network is able to identify a "sub-seasonal" evolution of subseasonal predictability sourced from the MJO and ENSO.

To ensure the network does not solely rely on DOY to classify confident predictions, we also train neural networks without DOY information, and find similar MJO and ENSO contribution results (not shown). To maximize samples, the following analysis examines predictions throughout the season, rather than only during the latter half of boreal winter.

## 3.2 MJO- & ENSO-Network Contributions

Due to the construction of the neural network, the relative contributions from each network to the final predictions can be quantified. Specifically, we calculate the frequency that either the ENSO- (teal) or MJO- (purple) network solely contributes to a correct, final prediction (Figure 3a). The frequency that both networks contribute to a correct prediction is also included in grey, so that the sum of the teal, purple and grey lines at a specific lead and Z500 averaging window is 100%. Lighter (darker) colors denote shorter (longer) temporal Z500 averaging windows.

Overall, we find that the ENSO-network alone (teal) contributes more frequently to correct predictions than the MJO-network alone (purple) for almost all leads and Z500 averaging windows. At shorter Z500 averaging windows (2 and 7 days), the MJO-network contributes more frequently until about a lead of 14-18 days, after which the ENSO-network becomes more frequently correct regardless of Z500 averaging windows. The most fre-

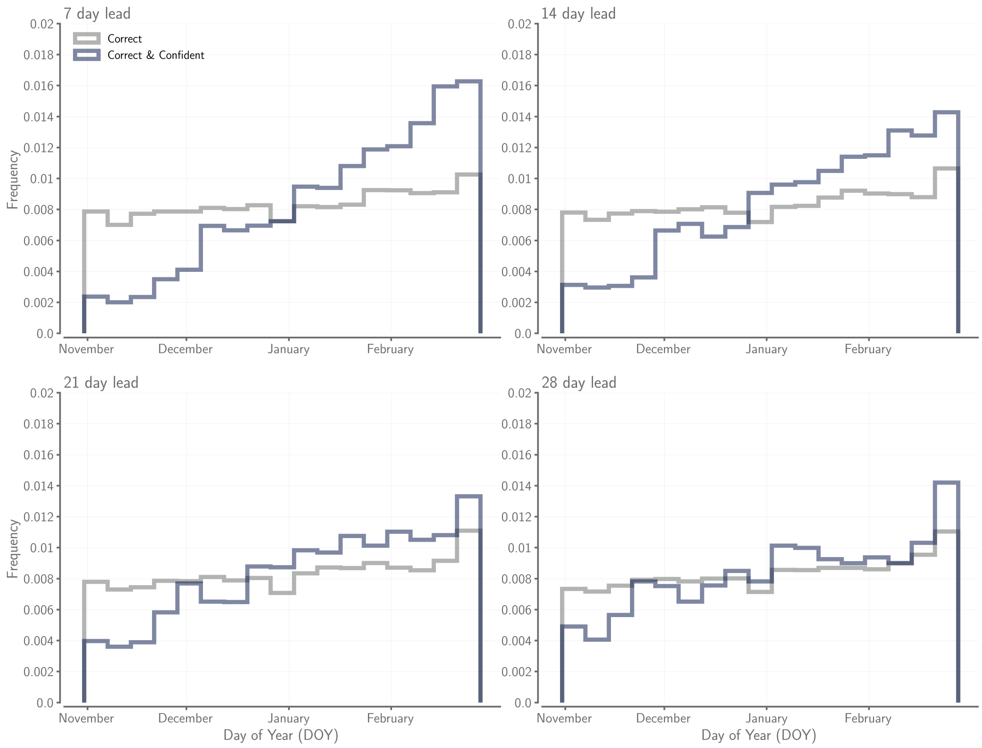


**Figure 2.** Frequency of a correct (grey) and confident (purple) network predictions by day of year (DOY) for a lead of 7, 14, 21, and 28 days across all Z500 averaging windows.

quently correct network combination is when *both* networks agree on the correct prediction (grey lines). However, the information provided by the ENSO state begins to contribute as frequently at leads greater than 21 days and longer averaging windows (darker teal lines). In general, as either the Z500 averaging window or lead time increases, the ENSO-network alone contributes more frequently to a correct prediction than the MJO-network. These results show that while the MJO-state is important for making predictions, ENSO plays a greater role in making correct subseasonal predictions for the majority of lead times and Z500 averaging windows.

If we further subset the predictions into correct and confident predictions (i.e. network-identified forecasts of opportunity), a similar though more exaggerated, story emerges. After a lead of 7 days, the ENSO-network contributes more frequently to correct and confident predictions than the MJO-network, regardless of Z500 averaging window (Figure 3b). At shorter leads the most frequent correct, confident predictions still occur when *both* the ENSO- and MJO-network correctly contribute to the predictions. However, the ENSO-network alone rivals these frequencies after a lead of 21 days. These results again demonstrate that the ENSO-network alone is generally more useful for correct (and confident) subseasonal predictions than the MJO-network.

When confident and correct predictions are further separated into positive and negative Z500 anomaly predictions, the contributions become more nuanced (Fig. 3b.1- b.2). For negative predictions, the ENSO-network more frequently contributes to correct, confident predictions than the MJO-network, regardless of lead time or averaging window. However, when examining positive predictions [note change to y-axis limits], the MJO-network alone contributes to correct, confident predictions more frequently than the ENSO-network at 5-7 day leads and Z500 averaging windows of 2 and 7 days (Fig. 3b.2). This

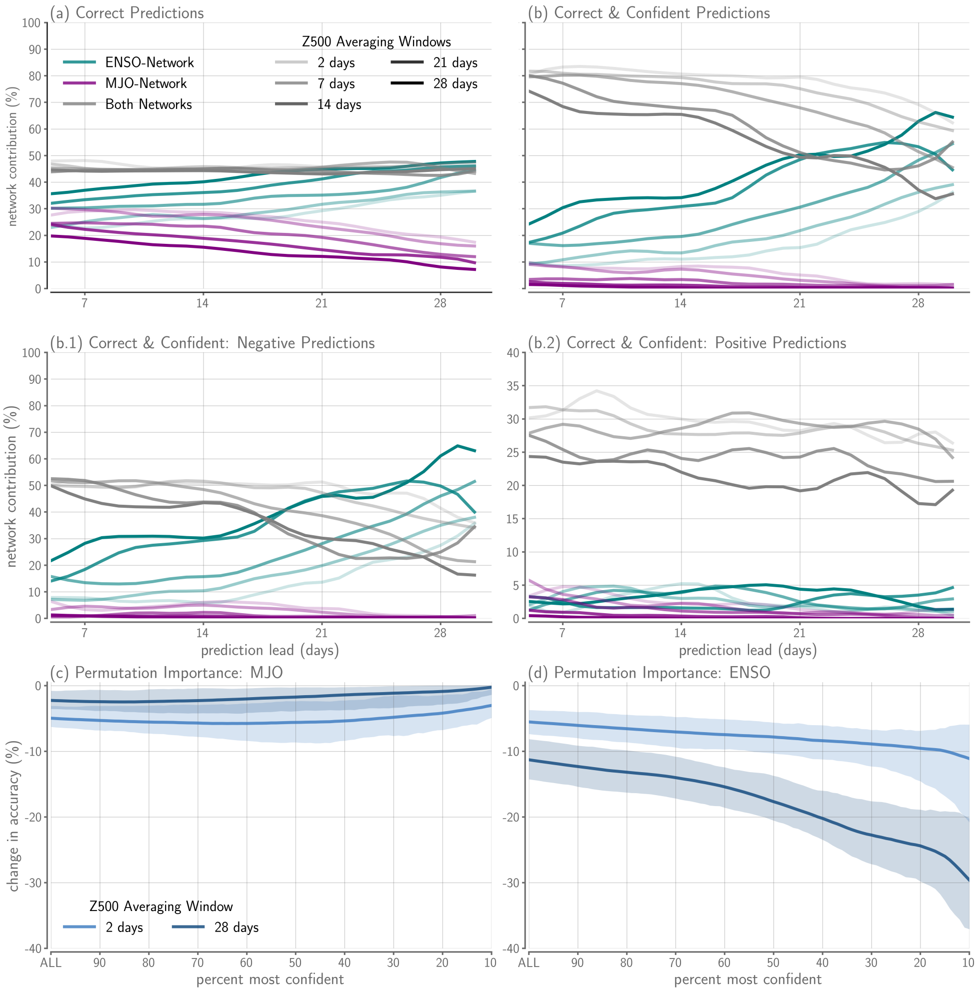


**Figure 3.** The frequency of a correct prediction provided by *either* the MJO- (purple) or ENSO-network (teal) or by *both* MJO- and ENSO-networks (grey) for each prediction lead. Lighter (darker) lines indicate shorter (longer) Z500 averaging windows. (b) As in (a) but for correct and confident predictions, which is further divided into (b.1) positive and (b.2) negative Z500 predictions [note different y-axis limits]. Lines are smoothed with a 3 day triangle filter for ease of interpretation. (c,d) Change in accuracy across confidence thresholds after permuting (c) RMM and (d) ENSO index input. The light/dark blue lines represent the mean of a 2 day/28 day Z500 averaging window across all lead times and the associated range of change in accuracy is represented by the shading.

suggests the MJO state is especially important for subseasonal prediction of anomalously high Z500 at shorter leads and averaging windows, particularly when the ENSO state is not useful (e.g. ENSO neutral conditions).

The utility of the MJO-network to the total network can be further elucidated when the prediction problem is, for example, constructed with a lead of 10 days and a Z500 averaging window of 5 days. We find that 42% of correct, confident positive Z500 anomaly predictions are periods with ENSO neutral conditions, when the tropical ocean should have the least control on the extratropical eastern Pacific. This is in stark contrast to confident, correct negative predictions which only occur in ENSO neutral states in 12% of cases. With that said, we note that negative predictions, of which the ENSO-network dominates, are overall more frequently confident and correct than positive predictions (Fig. 3b.1).

The results of the relative network contributions generally suggests the ENSO-network is the main contributor to correct (and confident) predictions. However, the MJO-network shows its utility for positive predictions when the network is correct and confident. We can further explore the impact of the MJO-network and ENSO-network on prediction skill through permutation importance (Figure 3c,d). In particular, we can quantify the contribution of the ENSO-network to the accuracy of the total network (Figure 3d) by randomly shuffling the input into the ENSO-network. In doing so, we separate the connection between the predictor and predictand, and thus, the predictors importance for making correct predictions. We find that across lead (shading) and Z500 averaging window (lines), the ENSO-network contributes between 5-12% for all predictions and close to 40% when the network is very confident. When permutation importance is instead applied to the MJO-network (Figure 3c), this contribution is about 1-5% across confident thresholds. We again only include the two extreme Z500 averaging windows for visualization, however, the other averaging window results lie within these curves. This further demonstrates that information provided by the ENSO-network is more important for higher skill, particularly at high confidence values (i.e. during forecasts of opportunity), compared to the MJO-network.

#### *3.2.1 MJO-Network Importance*

In general, our network indicates that ENSO is a more consistent provider of forecast skill of Z500 anomalies over the North Pacific. Nevertheless, there are specific time frames when the MJO-network provides important information for predicting Z500. To delve deeper into the MJO's optimal state for subseasonal predictability of Z500 in the North Pacific, K-means clustering is employed on the input features of the MJO network (RMM1 and RMM2). For brevity, we focus on a single lead time and averaging window (10 days and 5 days, respectively). This was found as a lead time and averaging window of relative peak importance for MJO driven predictability (Fig. 3b). This analysis focuses on instances when the network is confident and accurate, only during neutral ENSO conditions. We employ elbow and silhouette analysis to ascertain the optimal number of clusters for both positive and negative confident and correct predictions (Fig. S2, Rousseeuw, 1987). These methods offer a quantitative measure of how well-defined and separated the clusters are, providing insights into the cohesion within each cluster and the distinctiveness between clusters. This ensures a more nuanced evaluation of the clustering structure and reinforces our confidence in the appropriateness of the chosen number of clusters (3; Figure S2). The silhouette analysis shows clearly separated clusters which enhances the reliability of our clustering results, contributing to the overall robustness of our analysis. We then take a mean across the temporal dimension of each cluster to form a cluster composite of the input MJO RMM1/RMM2 predictor variables. Composites of the three clusters, for positive (top row) and negative (bottom row) Z500 anomaly predictions, are shown in figure 4.

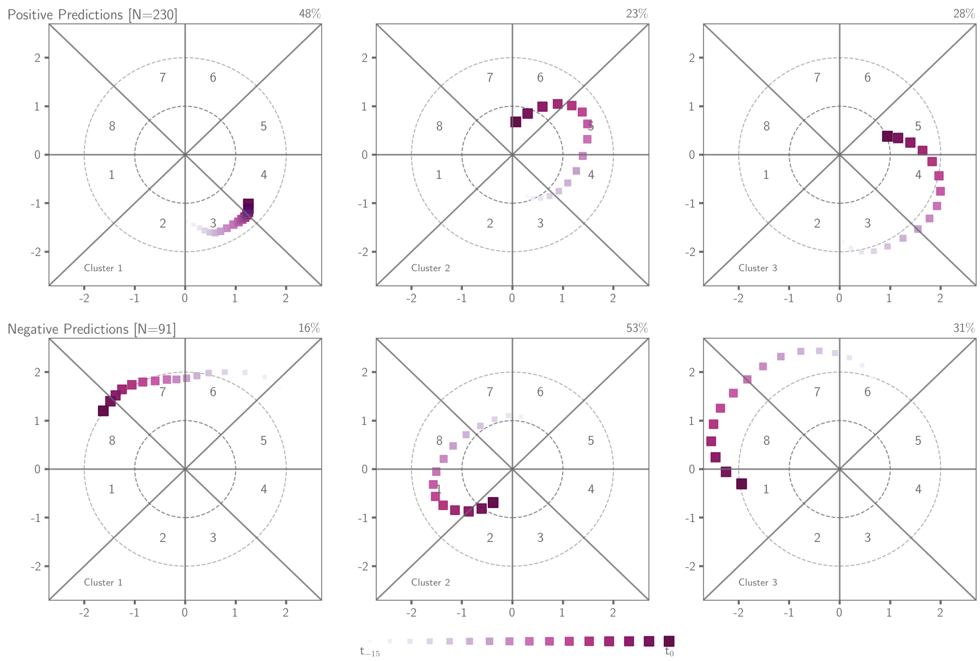


**Figure 4.** Composite clusters of MJO events when predictions are confident, correct, and ENSO is in a neutral state for anomalously high (top row) and anomalously low (bottom row) Aleutian Low states. Forecast lead is 10 days and a Z500 averaging window of 5 days. The RMM indices progress in time from light- $[t_{-15}]$ to dark- $[t_0]$ colors.

Firstly, we observe the frequency of events in which ENSO is neutral and the network exhibits both confident and correct predictions, represented as an N value in each row. Positive predictions are approximately 2.5 times more likely than negative events to exhibit this forecast condition (N=230 vs. N=91). This implies that the network demonstrates greater confidence and accuracy when forecasting positive Z500 anomalies during ENSO neutral states. Consequently, the MJO proves to be a more effective predictor (in CESM2-PI) in phases 3/4, where downstream Rossby wave dispersion leads to positive Z500 North Pacific anomalies. It is important to note that this does not necessarily imply that positive anomalies are universally more predictable at the subseasonal range, as the total number of confident, correct negative predictions is higher than those predicting a positive state (refer to the discussion of Fig. 3 for further details), and this is largely driven by ENSO positive events.

Positive predictions (row 1; high Z500 anomalies) show three distinct developing MJO states. Each developing MJO state is consistent with the phases that lead to a downstream positive Z500 anomaly (peaking in phases 3/4/5), demonstrating that the neural network has identified a physically justifiable link between the MJO and North Pacific circulation. Every cluster is above the threshold for active MJO events (1 sigma, inner dashed circle), and cluster 3 has periods which are above the 2 standard deviation threshold (97.5 percentile; outer dashed circle). Meaning, extremely anomalous events more consistently produce downstream extra-tropical Z500 anomalies. Cluster 1 shows a persistent anomaly in which the MJO stalls in between phases 3 and 4. These persistent cases have been previously identified as exciting a greater teleconnection response than fast moving MJO events (Yadav & Straus, 2017; Yadav et al., 2024). Finally, clusters 2 and 3 show events that are anomalously strong which then decay into MJO neutral states as they move towards initialization time. This is logical as MJO phase 6/7/8 is associated with a negative Z500 anomaly and thus would negate the current Z500 positive prediction at subseasonal forecast leads. To the author's knowledge, this is a unique aspect of this analysis showing that selective extremely anomalous MJO phases which then decay to a neutral MJO state can lead to enhanced subseasonal forecast skill, by *not* sparking MJO induced Rossby wave destructive interference. For the sake of brevity, we will simply note that the negative Z500 predictions (row2; low Z500 anomalies), largely mirror the findings found in the positive Z500 predictions.

The authors acknowledge that the MJO and ENSO indices along with the day of year are the sole information available to the network for making predictions. Keeping this limitation in mind, in summary, the subseasonal predictability of the Eastern North Pacific Z500 anomaly is predominantly influenced by highly active or persistent MJO events during neutral ENSO conditions. Larger anomalies result in increased predictability, and MJO events with substantial anomalies that subsequently transition into neutral states significantly contribute to subseasonal forecast skill.

## 4 Conclusion

This study aims to use an interpretable neural network to enhance the scientific understanding of the contribution of two tropical modes of variability to subseasonal predictability over the North Pacific: the MJO and ENSO. We find the network performs well on both the CESM2-PI testing data and ERA5 reanalysis across the range of lead time and averaging windows evaluated, suggesting the network is able to identify physically relevant sources of predictability. Further, the network is able to identify a late boreal winter preference for enhanced subseasonal predictability (Fig. 2), consistent with previous research which explores the importance of the subseasonal evolution of the background state for teleconnection propagation (e.g., Kumar & Hoerling, 1998; Chapman et al., 2021). This area of predictability research remains relatively unexplored, calling for more focused investigation.

Through an analysis of the relative roles of the MJO- and ENSO-networks, we find that forecast lead time and predictand averaging windows have a limited effect on the relative importance of MJO-driven North Pacific variability. ENSO dominates as the primary driver of subseasonal predictability for the majority of lead times and averaging windows, particularly at forecast ranges exceeding 7 days and averaging windows greater than 2 days (Fig. 3b,d). However, the MJO does provide some utility for prediction of positive Z500 anomalies during ENSO neutral states. In particular, persistent and particularly anomalous MJO events that decay before creating destructive interference offer the greatest utility for subseasonal predictability from the MJO in this region (Fig. 4).

The authors acknowledge that we predict the *sign* of the Aleutian Low anomaly and the relative importance of each predictor variable could change if the predictive target is changed to forecasting the magnitude or other, downstream affects of the MJO or ENSO (i.e., two-meter temperature or precipitation). Further, these results are for the CESM2-PI simulation, and therefore, does not account for possible affects from anthropogenic climate change. Recent research has shown that the MJO has become and will likely continue to become more predictable in a future climate (Du et al., 2023), which could subsequently improve midlatitude subseasonal skill provided by the MJO. On the other hand, previous research suggests ENSO may be the main tropical driver of future midlatitude subseasonal predictability changes (Mayer & Barnes, 2022). Therefore, future research should explore how our results may change in a future, warmer climate.

Given the chaotic nature of the weather system, a priori identification of particularly predictive windows offers a useful way forward for long range forecast skill (Albers & Newman, 2019; Mariotti et al., 2020). Ultimately, this paper demonstrates that interpretable neural networks can be used to gain physical insight into predictability, particularly through dissecting the relative importance of modes of variability thought important for subseasonal predictability.

## 5 Open Research

To promote transparency and reproducibility, all model training scripts and figures are readily accessible and can be downloaded using the provided code available on GitHub (https://github.com/kjmayer/ENSOvsMJO ; Mayer & Chapman, 2024). Comprehensive instructions for each step of this study are documented in the repository's README file. The authors leveraged the TensorFlow Python toolbox for machine learning and model training, a python machine learning environment can be found in this projects' repository. All data was produced as a part of the Community Earth System Model's contribution to the CMIP6 suite and is archived at the U.S. National Science Foundation's National Center for Atmospheric Research (NSF NCAR) computational and information systems lab (https://www2.cisl.ucar.edu/computing-data/data/cmip6-data-sets-glade). Raw ERA5 Reanalysis data can be obtained on the NSF NCAR Research Data Archive at: https://rda.ucar.edu/datasets/ds633.0/. Intermediate data files that can be leveraged to run every neural network and produce every plot specified in the github repo are stored at NCAR's Geoscience Data Exchange (Chapman & Mayer, 2024).

**Acknowledgments**

The work conducted by KJM is supported by the U.S. Department of Energy, Office of Science, Office of Biological & Environmental Research (BER), Regional and Global Model Analysis (RGMA) component of the Earth and Environmental System Modeling Program under Award Number DE-SC0022070 and National Science Foundation (NSF) IA 1947282. WEC received M²LInES research funding by the generosity of Eric and Wendy Schmidt by recommendation of the Schmidt Futures program. Further, this material is based upon work supported by the U.S. National Science Foundation under Grant No. AGS - 2230301 (NSF SOARS). Additionally, this work was supported by the U.S. National Science Foundation National Center for Atmospheric Research (NSF NCAR), which is a major facility sponsored by the NSF under Cooperative Agreement No. 1852977. Any opinions, findings, and conclusions or recommendations expressed in this material are those of the author(s) and do not necessarily reflect the views of the U.S. National Science Foundation.

We thank Dr. Emily Gordon for her insight and advice on using this interpretable neural networks.

## References

Agarwal, R., Melnick, L., Frosst, N., Zhang, X., Lengerich, B., Caruana, R., & Hinton, G. (2020, April). Neural additive models: Interpretable machine learning with neural nets.

Albers, J. R., & Newman, M. (2019). A priori identification of skillful extratropical subseasonal forecasts. *Geophysical Research Letters*, *46*(21), 12527–12536.

Arcodia, M. C., Kirtman, B. P., & Siqueira, L. S. P. (2020). How MJO teleconnections and ENSO interference impacts US precipitation. *J. Clim.*.

Capotondi, A., Deser, C., Phillips, A., Okumura, Y., & Larson, S. (2020). Enso and pacific decadal variability in the community earth system model version 2. *Journal of Advances in Modeling Earth Systems*, *12*(12), e2019MS002022.

Chapman, W. E., & Mayer, K. J. (2024). *Data for Exploring the Relative Contribution of the MJO and ENSO to Midlatitude Subseasonal Predictability [Dataset].* doi: https://doi.org/10.5065/f21v-ya03

Chapman, W. E., Subramanian, A. C., Xie, S.-P., Sierks, M. D., Ralph, F. M., & Kamae, Y. (2021). Monthly modulations of enso teleconnections: Implications for potential predictability in north america. *Journal of Climate*, *34*(14), 5899–5921.

Danabasoglu, G., Lamarque, J.-F., Bacmeister, J., Bailey, D., DuVivier, A., Edwards, J., ... others (2020). The community earth system model version 2 (cesm2). *Journal of Advances in Modeling Earth Systems*, *12*(2), e2019MS001916.

Davenport, F. V., & Diffenbaugh, N. S. (2021, July). Using machine learning to analyze physical causes of climate change: A case study of U.S. midwest extreme precipitation. *Geophys. Res. Lett.*.

Du, D., Subramanian, A. C., Han, W., Chapman, W. E., Weiss, J. B., & Bradley, E. (2023). Increase in mjo predictability under global warming. *Nature Climate Change*, 1–7.

Feldstein, S. B. (2002). Fundamental mechanisms of the growth and decay of the pna teleconnection pattern. *Quarterly Journal of the Royal Meteorological Society: A journal of the atmospheric sciences, applied meteorology and physical oceanography*, *128*(581), 775–796.

Frederiksen, J. (1983). A unified three-dimensional instability theory of the onset of blocking and cyclogenesis. ii. teleconnection patterns. *Journal of Atmospheric Sciences*, *40*(11), 2593–2609.

Gibson, P. B., Chapman, W. E., Altinok, A., Delle Monache, L., DeFlorio, M. J., & Waliser, D. E. (2021). Training machine learning models on climate model output yields skillful interpretable seasonal precipitation forecasts. *Communications Earth & Environment*, *2*(1), 159.

Gordon, E. M., Barnes, E. A., & Davenport, F. V. (2023). Separating internal and forced contributions to near term sst predictability in the cesm2-le. *Environmental Research Letters*.

Gordon, E. M., Barnes, E. A., & Hurrell, J. W. (2021, November). Oceanic harbingers of pacific decadal oscillation predictability in CESM2 detected by neural networks. *Geophys. Res. Lett.*, *48*(21).

Henderson, S. A., & Maloney, E. D. (2018, July). The impact of the Madden–Julian oscillation on High-Latitude winter blocking during el niño–southern oscillation events. *J. Clim.*, *31*(13), 5293–5318.

Henderson, S. A., Maloney, E. D., & Barnes, E. A. (2016). The influence of the madden–julian oscillation on northern hemisphere winter blocking. *Journal of Climate*, *29*(12), 4597–4616.

Hendon, H. H., Zhang, C., & Glick, J. D. (1999, August). Interannual variation of the Madden–Julian oscillation during austral summer. *J. Clim.*, *12*(8), 2538–2550.

Hersbach, H., Bell, B., Berrisford, P., Hirahara, S., Horányi, A., Muñoz-Sabater, J., ... others (2020). The era5 global reanalysis. *Quarterly Journal of the Royal Meteorological Society*, *146*(730), 1999–2049.

Hoskins, B. J., & Ambrizzi, T. (1993, June). Rossby wave propagation on a realistic longitudinally varying flow. *J. Atmos. Sci.*, *50*(12), 1661–1671.

Johnson, N. C., Collins, D. C., Feldstein, S. B., L'Heureux, M. L., & Riddle, E. E. (2014, February). Skillful wintertime north american temperature forecasts out to 4 weeks based on the state of ENSO and the MJO. *Weather Forecast.*, *29*(1), 23–38.

Johnson, N. C., Collins, D. C., Feldstein, S. B., L'Heureux, M. L., & Riddle, E. E. (2014). Skillful wintertime north american temperature forecasts out to 4 weeks based on the state of enso and the mjo. *Weather and Forecasting*, *29*(1), 23–38.

Kessler, W. S. (2001, July). EOF representations of the Madden–Julian oscillation and its connection with ENSO. *J. Clim.*, *14*(13), 3055–3061.

Kingma, D. P., & Ba, J. (2014). Adam: A method for stochastic optimization. *arXiv preprint arXiv:1412.6980*.

Kumar, A., & Hoerling, M. P. (1998). Annual cycle of pacific–north american seasonal predictability associated with different phases of enso. *Journal of Climate*, *11*(12), 3295–3308.

Labe, Z. M., & Barnes, E. A. (2022, May). Predicting slowdowns in decadal climate warming trends with explainable neural networks. *Geophys. Res. Lett.*.

Lin, H., Brunet, G., & Derome, J. (2008). Forecast skill of the madden–julian oscillation in two canadian atmospheric models. *Monthly Weather Review*, *136*(11), 4130–4149.

Madden, R. A., & Julian, P. R. (1971, July). Detection of a 40–50 day oscillation in the zonal wind in the tropical pacific. *J. Atmos. Sci.*, *28*(5), 702–708.

Madden, R. A., & Julian, P. R. (1972, September). Description of Global-Scale circulation cells in the tropics with a 40–50 day period. *J. Atmos. Sci.*, *29*(6), 1109–1123.

Madden, R. A., & Julian, P. R. (1994, May). Observations of the 40–50-day tropical Oscillation—A review. *Mon. Weather Rev.*, *122*(5), 814–837.

Mariotti, A., Baggett, C., Barnes, E. A., Becker, E., Butler, A., Collins, D. C., … Albers, J. (2020, January). Windows of opportunity for skillful forecasts subseasonal to seasonal and beyond. *Bull. Am. Meteorol. Soc.*.

Martin, Z. K., Barnes, E. A., & Maloney, E. (2022, May). Using simple, explainable neural networks to predict the Madden-Julian oscillation. *J. Adv. Model. Earth Syst.*.

Mayer, K. J., & Barnes, E. A. (2021, May). Subseasonal forecasts of opportunity identified by an explainable neural network. *Geophys. Res. Lett.*.

Mayer, K. J., & Barnes, E. A. (2022, July). Quantifying the effect of climate change on midlatitude subseasonal prediction skill provided by the tropics. *Geophys. Res. Lett.*, *49*(14).

Mayer, K. J., & Chapman, W. E. (2024). *Code (Version 1.0.0) for Exploring the Relative Contribution of the MJO and ENSO to Midlatitude Subseasonal Predictability [Software]. Zenodo.* Retrieved from `https://github.com/kjmayer/ENSOvsMJO` doi: https://doi.org/10.5281/zenodo.10607685

McGovern, A., Lagerquist, R., Gagne, D. J., Jergensen, G. E., Elmore, K. L., Homeyer, C. R., & Smith, T. (2019). Making the black box more transparent: Understanding the physical implications of machine learning. *Bulletin of the American Meteorological Society*, *100*(11), 2175–2199.

Merryfield, W. J., Baehr, J., Batté, L., & others. (2020). Current and emerging developments in subseasonal to decadal prediction. *Bulletin of the*.

Moon, J.-Y., Wang, B., & Ha, K.-J. (2011, September). ENSO regulation of MJO teleconnection. *Clim. Dyn.*, *37*(5), 1133–1149.

Namias, J. (1986, July). Persistence of flow patterns over north america and adjacent ocean sectors. *Mon. Weather Rev.*, *114*(7), 1368–1383.

Newman, M., & Sardeshmukh, P. D. (1998). The impact of the annual cycle on the north pacific/north american response to remote low-frequency forcing. *Journal of the Atmospheric Sciences*, *55*(8), 1336–1353.

Philander, S. (1985). El niño and la niña. *Journal of Atmospheric Sciences*, *42*(23), 2652–2662.

Pohl, B., & Matthews, A. J. (2007, June). Observed changes in the lifetime and amplitude of the Madden–Julian oscillation associated with interannual ENSO sea surface temperature anomalies. *J. Clim.*, *20*(11), 2659–2674.

Rousseeuw, P. J. (1987). Silhouettes: a graphical aid to the interpretation and validation of cluster analysis. *Journal of computational and applied mathematics*, *20*, 53–65.

Sardeshmukh, P. D., & Hoskins, B. J. (1988). The generation of global rotational flow by steady idealized tropical divergence. *Journal of the Atmospheric Sciences*, *45*(7), 1228–1251.

Simmons, A., Wallace, J., & Branstator, G. (1983). Barotropic wave propagation and instability, and atmospheric teleconnection patterns. *Journal of the Atmospheric Sciences*, *40*(6), 1363–1392.
Stan, C., Straus, D. M., Frederiksen, J. S., Lin, H., Maloney, E. D., & Schumacher, C. (2017, December). Review of Tropical-Extratropical teleconnections on intraseasonal time scales: The subseasonal to seasonal (S2S) teleconnection Sub-Project. *Rev. Geophys.*, *55*(4), 902–937.
Takahashi, C., & Shirooka, R. (2014, September). Storm track activity over the north pacific associated with the Madden-Julian oscillation under ENSO conditions during boreal winter. *J. Geophys. Res.*, *119*(18), 10,663–10,683.
Toms, B. A., Barnes, E. A., & Ebert-Uphoff, I. (2020, September). Physically interpretable neural networks for the geosciences: Applications to earth system variability. *J. Adv. Model. Earth Syst.*, *12*(9).
Toms, B. A., Kashinath, K., Yang, D., & Prabhat. (2021, July). Testing the reliability of interpretable neural networks in geoscience using the Madden–Julian oscillation. *Geosci. Model Dev.*, *14*(7), 4495–4508.
Trenberth, K. E. (1997). The definition of el nino. *Bull. Am. Meteorol. Soc.*, *78*(12), 2771–2778.
Tseng, K.-C., Barnes, E. A., & Maloney, E. D. (2018, January). Prediction of the midlatitude response to strong Madden-Julian oscillation events on S2S time scales: PREDICTION OF Z500 AT S2S TIME SCALES. *Geophys. Res. Lett.*, *45*(1), 463–470.
Tseng, K.-C., Maloney, E., & Barnes, E. A. (2020, May). The consistency of MJO teleconnection patterns on interannual time scales. *J. Clim.*, *33*(9), 3471–3486.
Vitart, F., Ardilouze, C., Bonet, A., Brookshaw, A., Chen, M., Codorean, C., … Zhang, L. (2017, January). The subseasonal to seasonal (S2S) prediction project database. *Bull. Am. Meteorol. Soc.*, *98*(1), 163–173.
Vitart, F., Robertson, A. W., & Anderson, D. L. T. (2012, January). Subseasonal to seasonal prediction project: Bridging the gap between weather and climate. *WMO Bull.*, *61*(61).
Wallace, J. M., & Gutzler, D. S. (1981). Teleconnections in the geopotential height field during the northern hemisphere winter. *Monthly weather review*, *109*(4), 784–812.
Wang, J., Kim, H., & DeFlorio, M. J. (2022). Future changes of pna-like mjo teleconnections in cmip6 models: Underlying mechanisms and uncertainty. *Journal of Climate*, *35*(11), 3459–3478.
Wang, L., & Robertson, A. W. (2019, May). Week 3–4 predictability over the united states assessed from two operational ensemble prediction systems. *Clim. Dyn.*, *52*(9), 5861–5875.
Wheeler, M. C., & Hendon, H. H. (2004). An all-season real-time multivariate mjo index: Development of an index for monitoring and prediction. *Monthly weather review*, *132*(8), 1917–1932.
White, C. J., Carlsen, H., Robertson, A. W., Klein, R. J. T., Lazo, J. K., Kumar, A., … Zebiak, S. E. (2017, July). Potential applications of subseasonal-to-seasonal (S2S) predictions. *Met. Apps*, *24*(3), 315–325.
White, C. J., Domeisen, D. I. V., Acharya, N., Adefisan, E. A., Anderson, M. L., Aura, S., … Wilson, R. G. (2021, November). Advances in the application and utility of subseasonal-to-seasonal predictions. *Bull. Am. Meteorol. Soc.*, *-1*(aop), 1–57.
Winkler, C. R., Newman, M., & Sardeshmukh, P. D. (2001). A linear model of wintertime low-frequency variability. part i: Formulation and forecast skill. *Journal of climate*, *14*(24), 4474–4494.
Yadav, P., Garfinkel, C. I., & Domeisen, D. I. (2024). The role of the stratosphere in teleconnections arising from fast and slow mjo episodes. *Geophysical Research Let-*

*ters*, *51* (1), e2023GL104826.

Yadav, P., & Straus, D. M. (2017). Circulation response to fast and slow mjo episodes. *Monthly Weather Review*, *145* (5), 1577–1596.

Zhuang, J., Dussin, R., Jüling, A., & Rasp, S. (2018). xesmf: Universal regridder for geospatial data. *Zenodo [code]*, *10*.

# Exploring the Relative Contribution of the MJO and ENSO to Midlatitude Subseasonal Predictability

**Kirsten J. Mayer[1*], William E. Chapman[1*], William A. Manriquez[2]**

[1]U.S. National Science Foundation National Center for Atmospheric Research
[2]Metropolitan State University of Denver
[*]These authors contributed equally

**Key Points:**

- An interpretable neural network is used to decompose contributions of MJO and ENSO to North Pacific subseasonal circulation predictability.
- ENSO alone is overall more useful than the MJO for subseasonal predictions across various lead times and predictand averaging windows.
- Unique MJO events, that provide enhanced subseasonal predictability during ENSO neutral conditions, are identified.

Corresponding authors: Kirsten J. Mayer; William E. Chapman, `kjmayer@ucar.edu; wchapman@ucar.edu`

## Abstract

Here we explore the relative contribution of the Madden-Julian Oscillation (MJO) and El Niño Southern Oscillation (ENSO) to midlatitude subseasonal predictive skill of upper atmospheric circulation over the North Pacific, using an inherently interpretable neural network applied to pre-industrial control runs of the Community Earth System Model version 2. We find that this interpretable network generally favors the state of ENSO, rather than the MJO, to make correct predictions on a range of subseasonal lead times and predictand averaging windows. Moreover, the predictability of positive circulation anomalies over the North Pacific is comparatively lower than that of their negative counterparts, especially evident when the ENSO state is important. However, when ENSO is in a neutral state, our findings indicate that the MJO provides some predictive information, particularly for positive anomalies. We identify three distinct evolutions of these MJO states, offering fresh insights into opportune forecasting windows for MJO teleconnections.

## Plain Language Summary

Weather is hard to predict with longer forecast leads. Here, we use a data-driven statistical model to dissect tropical sources of predictability on 2 week to 2 month midlatitude upper-level variability. This model was constructed so that we can identify the relative contributions of two tropical phenomena important for predictability on these timescales. Namely, we use the Madden-Jullian Oscillation (MJO) and the El Niño Southern Oscillation (ENSO) as predictor variables, two phenomena that provide a teleconnecting signal from the tropics to midlatitude variability. We find that the ENSO signal alone consistently provides more forecast predictability than the MJO. However, when ENSO is not active, the MJO provides distinct windows of forecast opportunity, particularly for anomalously anticyclonic events. We identify three evolutions of the MJO which offer new insights into forecasting weather at long forecast leads.

## 1 Introduction

Forecasting for the subseasonal timescale (often defined as 2 weeks through 2 months) has received considerable attention over the last decade (White et al., 2017; Mariotti et al., 2020; Merryfield et al., 2020; White et al., 2021). These timescales are particularly difficult to predict as generally neither atmospheric initial conditions nor slower varying boundary conditions provide sufficient information to make useful predictions (Vitart et al., 2012, 2017; Mariotti et al., 2020). Unfortunately, this is also a timescale in which many public and private sectors seek information to make informed, actionable decisions in order to save lives and property (White et al., 2017, 2021). One way to garner skill on these timescales is to harness predictive skill from specific modes of variability known to provide enhanced subseasonal predictability when the mode is active – termed forecasts of opportunity (Mariotti et al., 2020). One such mode of variability that has gathered considerable attention in the subseasonal community is the Madden-Julian Oscillation (MJO; Madden & Julian, 1971, 1972, 1994).

The MJO consists of two oppositely signed zonally oriented convective anomalies that propagate from the Indian Ocean to the central Pacific, completing a cycle every 20 to 90 days. The associated upper-level circulation anomalies can interact with the subtropical jet, exciting quasi-stationary Rossby waves (Hoskins & Ambrizzi, 1993), which influence midlatitude circulation anomalies on subseasonal timescales. Following specific phases (i.e. locations) of the MJO, this teleconnection can lead to improved prediction skill on subseasonal timescales (Tseng et al., 2018). The MJO teleconnection has been shown to manifest as a Pacific North American (PNA) - like system. In its positive phase, the PNA is characterized by a deepened Aleutian Low, and increased Canadian High, and a deepened Florida low pattern which extends into the Atlantic (Wallace & Gutzler, 1981). The Aleutian Low limb of the PNA, in particular, is responsible for greater downstream effects of precipitation and temperature anomalies across the whole of North America. In observations, the growth of the PNA anomaly is dominated by barotropic energy conversion from the zonally asymmetric climatological flow in the North Pacific storm track (e.g., Feldstein, 2002; Frederiksen, 1983; Simmons et al., 1983). However, a primary mode of Aleutian Low growth is also from excitation by tropical heating, such as from the MJO or El Niño Southern Oscillation (ENSO) Hoskins & Ambrizzi (1993); Sardeshmukh & Hoskins (1988).

ENSO is an interannual coupled ocean-atmosphere mode in the tropical Pacific (Trenberth, 1997), and the primary mode of tropical variability. However, it can also influence the subseasonal timescale through its impact on the MJO (Hendon et al., 1999; Kessler, 2001; Pohl & Matthews, 2007) and the basic state in which MJO teleconnections propagate (Namias, 1986; Moon et al., 2011; Takahashi & Shirooka, 2014), ultimately impacting the MJO's influence in the midlatitudes (Stan et al., 2017; Henderson & Maloney, 2018; Tseng et al., 2020; Arcodia et al., 2020) and subsequent subseasonal prediction skill (Johnson, Collins, Feldstein, L'Heureux, & Riddle, 2014; L. Wang & Robertson, 2019). Further, recent work suggests ENSO may play a main role in changes to midlatitude subseasonal predictability in a future, warmer climate (Mayer & Barnes, 2022). While ENSO is often used for seasonal prediction (e.g., Gibson et al., 2021; Winkler et al., 2001), there is also considerable literature that highlights ENSO teleconnections as a driver of midlatitude subseasonal variability, particularly in boreal winter by also modulating the Aleutian Low (e.g., Kumar & Hoerling, 1998; Chapman et al., 2021). Notably, the ENSO teleconnection exhibits significant evolution throughout a season. This dynamic evolution contributes to heightened predictability and diverse surface responses, contingent on the time of year and the strength of the background flow (the mid-latitude jet). Consequently, this lends support to the suggestion that ENSO could rival the MJO as a dominant driver of subseasonal forecast skill (Chapman et al., 2021).

These results raise the question as to the relative role of the MJO and ENSO in midlatitude subseasonal predictability. Johnson, Collins, Feldstein, L'Heureux, & Riddle (2014) showed that skillfull subseasonal forecasts can be derived solely using the state of the MJO and ENSO. However, given the time-scale of these two modes of variability, the utility of the MJO for midlatitude predictability dwindles as a function of leadtime while the ENSO utility remains a reliable source of longer range predictability. This study seeks to further elucidate the relative roles of both ENSO and MJO for midlatitude subseasonal forecasting using a more complex and interpretable statistical technique. We explore a range of forecast lead times and predictand averaging window lengths to investigate the relative role of these tropical drivers of subseasonal predictability for a variety of forecast criteria.

In recent years, neural networks have been shown to be a powerful statistical tool for the atmospheric sciences due to their ability to identify non-linear, physical relationships within large amounts of data (Toms et al., 2020, 2021; Labe & Barnes, 2022; Martin et al., 2022; Davenport & Diffenbaugh, 2021; Gordon et al., 2021). For example, on subseasonal timescales, explainable neural networks were demonstrated to identify subseasonal forecasts of opportunity using the network's "confidence" in a given prediction as well as the associated tropical sources of predictability through explainability techniques (Mayer & Barnes, 2021). Here we utilize network confidence and an interpretable neural network architecture known as a Neural Additive Model (Agarwal et al., 2020; Gordon et al., 2023), to disentangle the relative contributions of the MJO and ENSO to subseasonal predictability over the North Pacific in the pre-industrial control simulations from the Community Earth System Model. Specifically, we create two artificial neural networks, one of which receives an MJO index while the other receives an ENSO index. The predictions from these two networks are linearly combined to generate the final prediction for the sign of Z500 anomaly over the North Pacific on subseasonal timescales. This allows for the decomposition of a network's prediction into the respective contributions from ENSO and MJO. We find that information about the state of ENSO alone is overall more important than that of the MJO for subseasonal predictability of North Pacific circulation in the pre-industrial simulations. However, the state of the MJO still provides important information particularly for shorter lead time predictions of positive Z500 anomalies during network-identified forecasts of opportunity.

## 2 Data & Methods

### 2.1 Data

We leverage the Community Earth System Model version 2 (CESM2) pre-industrial control run (CESM2-PI) from model years 100-400 from the CMIP6 experiment suite (Danabasoglu et al., 2020). CESM2-PI has interactive land, coupled ocean with biogeochemistry, interacting sea-ice and non-evolving land ice, and constant 1850's CO2 forcing. The model's resolution is nominally 1 degree, with 32 vertical levels. A full description of the CESM2-PI runs can be found in Danabasoglu et al. (2020). From those years we select the daily geopotential height at 500 hpa (Z500), sea surface temperature (SST), and zonal wind at 200 hPa and 850 hPa (U200 and U850, respectively). We then separate the data into three independent data sets: training [model years 100-200], validation [model years 201-300], and testing [model years 301-400]. 100 years of training data was found sufficient to have the machine learning models fully converge on optimal solutions, meaning, adding more data did not significantly change resultant learned network weights. There is concensus that the eastern Pacific teleconnections associated with MJO and ENSO peak during the boreal winter (e.g., Philander, 1985; Henderson et al., 2016; Chapman et al., 2021). Therefore, we focus our investigation exclusively on this seasonal period, restricting our model training and analysis to input dates ranging from November 1st to February 28th. Consequently, the forecasts extend until March 30th, with a lead time of 30 days.

The practical relevance of this study relies on an accurate representation of the analyzed modes of variability in CESM2-PI. The primary rationale for scrutinizing predictability within CESM2-PI, rather than relying on observations, is to augment the size of the datasets used for training, testing, and validating the neural networks. CESM2-PI is recognized as a cutting-edge model, particularly in its representation of the MJO and ENSO, along with their associated North Pacific teleconnections. Numerous studies have evaluated the accuracy of this representation (Danabasoglu et al., 2020; J. Wang et al., 2022; Capotondi et al., 2020). To further corroborate the fidelity of these teleconnections, with particular attention to the task presented to the neural network, we present the frequency of anomalous Z500 signs 5-9 days after an active MJO in phases 3/4 and 6/7 in the supplementary material (Fig. S1), and compare that representation to that in ECMWF's version 5 reanalysis product (ERA5, Hersbach et al., 2020). It is clear that the model represents the MJO teleconnection well, capturing the dominate location and sign of the Z500 anomalous for the two active teleconnection phases of the MJO.

Additionally, the same suite of forecast variables was downloaded from ERA5 (1979-2020), to verify that the ML models results are valid on a global reanalysis product. The ERA5 product is regridded to the common CESM2 grid prior to any reanalysis using a bilinear interpolation scheme (Zhuang et al., 2018).

## 2.2 Methods

### *2.2.1 MJO, ENSO, & Aleutian Low Indices*

We follow the methods of Lin et al. (2008) for calculation of the real-time multivariate MJO indices (RMM1 and RMM2) in the CESM2-PI runs. Starting from the unfiltered observed daily averaged data of the OLR and zonal wind at 850-hPa and 200-hPa from model years 100-400, the time-mean, and the first three harmonics of the daily climatology are removed at every grid-point. Next, the time-series is filtered, by removing the grid-point time-mean of the previous 120 days. Removing the previous 120-day average eliminates most of the interannual variability, including the effects of ENSO. A meridional band average is then taken from 15°S to 15°N for the three fields. Each variable is then normalized by its own zonal average of temporal standard deviation, the fields are combined and decomposed and the two leading EOFs are retained. The resulting structures of the EOF modes are very similar to Wheeler & Hendon (2004, not shown).

The ENSO index is computed by employing a rolling 90-day window and a cosine latitude weighted average of the Sea Surface Temperature (SST) anomaly within the conventional Nino3.4 region [5°N-5°S and 170°W-120°W]. The SST anomaly is determined by subtracting a 60-day rolling average centered on each day of the year.

The target of the neural network is the sign of the Aleutian Low index. The Aleutian Low index is a representation the anomalous geopotential height at 500 hPa in the eastern North Pacific and is determined via the following process: Initially, a 60-day rolling average centered climatology is subtracted from the raw geopotential height data, with each center point corresponding the model day of year. Then the anomalous index within the target region [30°N to 60°N and 190°W to 250°W], is computed via a cosine latitude weighted average. Finally, the target averaging window is established by applying a forward rolling mean to the daily index data, using the desired target window length (2-28 days).

Finally, previous studies have indicated that the wintertime evolution of the basic state is non-trivial (Newman & Sardeshmukh, 1998) and thus tropically derived, eastern Pacific, teleconnections [which feed off the barotropic energy conversion provided by the divergence of the background jet] vary greatly (Chapman et al., 2021; Sardeshmukh & Hoskins, 1988). Thus, we also input the day of the year (DOY), which is represented as a linearly increasing value spanning from the first of November to the final day of February, encompassing all input days. The DOY index is subsequently normalized, ensuring it maintains a zero mean and a standard deviation of unity, prior to its incorporation into the neural network.

### *2.2.2 Interpretable Neural Network*

Figure 1 shows a schematic of the interpretable neural network specifically constructed to dissect the relative contributions of the MJO and ENSO to subseasonal predictability over the North Pacific. Following the general architecture laid out in Gordon et al. (2023), two artificial neural networks are combined at the output layer through a linear combination to create the final output prediction. In our applications, both networks are tasked to predict the sign of the 500 hPa geopotential height anomaly averaged over the North Pacific at the target lead. However, the top network (Figure 1a) only receives information about the state of ENSO and its evolution throughout 15 days prior (hereafter referred to as the ENSO-network) while the bottom network only receives the RMM1 and RMM2 index values and their evolution throughout the 15 days prior (Figure 1b; hereafter referred to as the MJO-network). Additionally, each network receives the DOY associated with $t_0$ as input so that it may also learn variability in sources of predictability within the boreal winter season. The final predictions are taken as the linear combination of the outputs of the individual networks, meaning that the network must learn

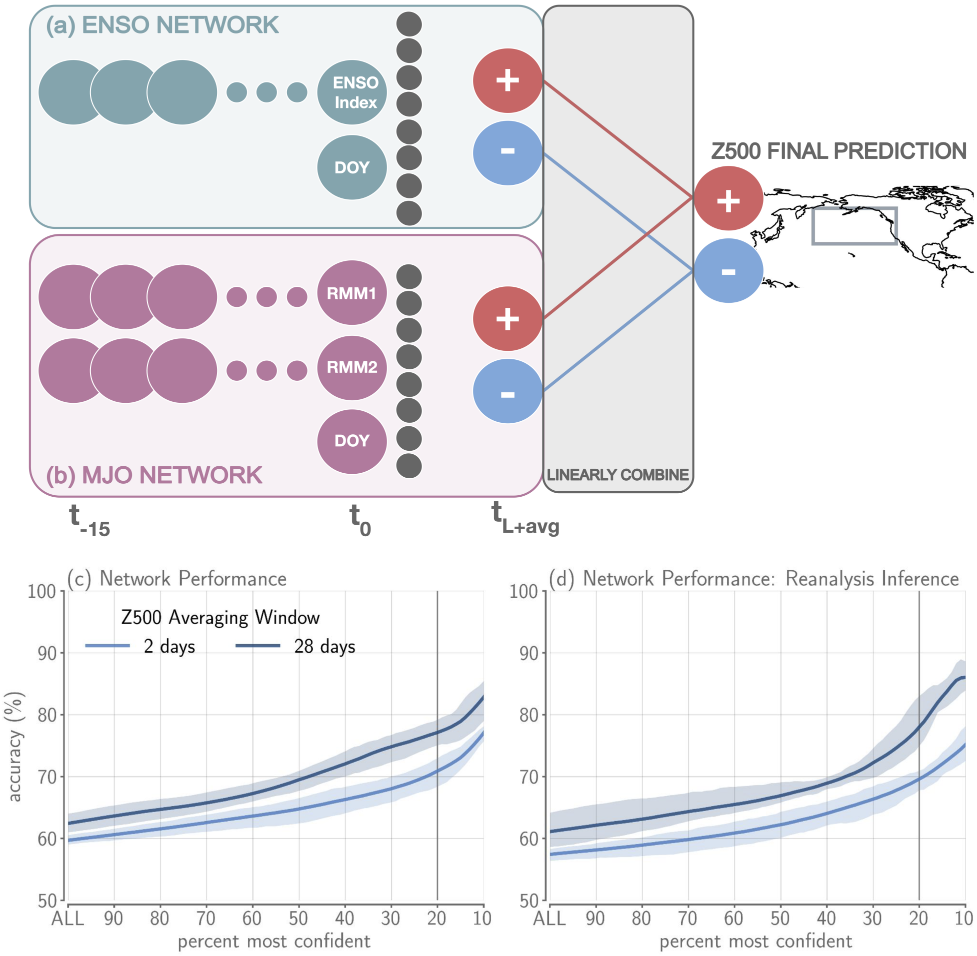


**Figure 1.** Schematic of the interpretable neural network architecture. Input into the (a) ENSO-network includes the ENSO index at $t_0$ plus the 15 days prior ($t_{-15}$) and associated normalized day of year (DOY) at $t_0$ to predict the sign of the Z500 anomaly averaged over North Pacific (grey rectangle) at a specified lead ($t_{L+avg}$, where "L" indicates the lead time and "avg" indicates the Z500 temporal averaging window length). The (b) MJO-network is constructed similarly but instead inputs RMM1 and RMM2 rather than the ENSO index. The predictions from each network are linearly combined (grey shaded box) to make the final network prediction. The bottom two panels include network performance [accuracy] across confidence thresholds for the (c) testing dataset and (d) ERA5 reanalysis. The light/dark blue lines represent the mean accuracy at each confidence level across all lead times (shading) for a Z500 averaging window of 2 days/28 days

to strategically weight its contribution to the final prediction. Therefore, the individual output of each neural network can be considered its contribution to a prediction, allowing interpretation of the specific role of each predictor (i.e., ENSO or MJO) in the network's skill.

To explore the impact of lead and predictand temporal averaging on the source of predictabilty, we train separate neural networks for leads ranging from 5 to 30 days and predictand temporal averaging windows of 2 to 28 days. Furthermore, we train five networks, each with a different random seed per lead and averaging window combination, to assess the network's sensitivity to random initialization weights. Minimal differences between random initializations are observed, leading us to present the results as averages across the five networks.

Both the ENSO- and MJO- networks have one hidden layer with eight nodes and use the rectified linear unit (ReLU) activation function. We note that increasing the complexity of either network does not impact the results [not shown]. To train the model, we use a batch size of 32, categorical crossentropy as the loss function and the Adam Optimizer (Kingma & Ba, 2014) for gradient descent with a learning rate of 0.001. The learning rate is initially held constant for the first 19 epochs and then reduced by 90% after each epoch to help minimize the loss. To reduce overfitting to the training data, training is completed after the validation loss does not improve for 20 epochs, at which time the network weights are reverted to 20 epochs prior. The softmax activation function is applied to the final layer of the total-network (Figure 1) so that the output values sum to one and represent a network estimation of likelihood, or "confidence". Previous research has shown that network confidence can be used to identify forecasts of opportunity when accuracy increases with confidence (Mayer & Barnes, 2021), allowing us to explore the contributions of the MJO and ENSO for all predictions and during network-identified forecasts of opportunity. Here, we define confident predictions as the 20% most confident following (Mayer & Barnes, 2022).

#### *2.2.3 Quantifying Relative Contribution*

We employ two methods to quantify the relative contribution of the ENSO- and MJO- networks to the total-network predictions. The first explores the frequency that the final, total prediction is correctly predicted by a specific network while incorrectly predicted by the other. This illuminates how often either the ENSO- *or* MJO- network solely contributes to the correct total-network prediction while the other network acts incorrectly.

The second metric quantifies the percentage of the total-network accuracy provided by either the ENSO- or MJO- network through permutation importance McGovern et al. (2019). Permutation importance is a technique used to remove relationships between the input and output through randomly shuffling the input data. The subsequent decrease in network performance can then be attributed to the importance of that input data to the prediction. To calculate the importance (percentage of accuracy) contributed by the ENSO-network, we randomly shuffle the ENSO index testing samples (retaining the 15 day memory), calculate the accuracy of the total-network with the randomly shuffled data, and compare it to the accuracy of the total-network without shuffled data. To calculate the percentage of accuracy contributed by the MJO-network, we apply the same technique, but shuffle the RMM indices. We note that the random shuffling does not account for memory between samples, and therefore, the network contribution to the total accuracy could be larger.

## 3 Results

### 3.1 Network Performance

To evaluate network performance, we calculate the accuracy of the network on the testing data across confidence levels (Figure 1c). The testing data is randomly subset to an equal number of positive and negative anomalies so that random chance is 50% for all predictions (N≈11,500; 100% most confident). Across the range of Z500 averaging windows (lines) and lead times (shading), the network performs better than random change at $\geq$ 60% accuracy. We include the two extreme averaging windows (2 and 28 days) for ease of visualization, however, the other averaging windows fall within these two curves. As network confidence increases, the accuracy of the network increases as well, indicating the network is able to identify periods of enhanced predictability (Figure 1c). Further, we find similar performance when the network is evaluated on reanalysis data (Figure 1d), suggesting the network is identifying physically relevant forecasts of opportunity for subseasonal predictability of Z500 anomalies over the North Pacific (Mayer & Barnes, 2021).

Previous work has also detailed the importance of the basic state evolution throughout boreal winter on tropically forced teleconnection propagation and its potential for improved subseasonal predictability (Newman & Sardeshmukh, 1998; Chapman et al., 2021, e.g.). Therefore, to account for any within season evolution of ENSO or MJO teleconnections to North Pacific predictability, DOY is included as an input into the network. We find that when the network is correct (grey histograms in Figure 2), the frequency of predictions are generally consistent across DOY with a slight increase towards the latter end of the season across leads 7 through 28 days. However, when the network is also confident (purple histograms in Figure 2), the frequency of predictions increases at the latter end of boreal winter. We note that the purple histograms become flatter with lead time (i.e. more early winter predictions) since longer lead time predictions made near the beginning of boreal winter are forecasting for the latter part of the season. These results indicate that the network has identified the latter half of boreal winter as a preferable period for enhanced subseasonal predictability, consistent with previous research (Newman & Sardeshmukh, 1998; Chapman et al., 2021). In other words, the network is able to identify a "sub-seasonal" evolution of subseasonal predictability sourced from the MJO and ENSO.

To ensure the network does not solely rely on DOY to classify confident predictions, we also train neural networks without DOY information, and find similar MJO and ENSO contribution results (not shown). To maximize samples, the following analysis examines predictions throughout the season, rather than only during the latter half of boreal winter.

### 3.2 MJO- & ENSO-Network Contributions

Due to the construction of the neural network, the relative contributions from each network to the final predictions can be quantified. Specifically, we calculate the frequency that either the ENSO- (teal) or MJO- (purple) network solely contributes to a correct, final prediction (Figure 3a). The frequency that both networks contribute to a correct prediction is also included in grey, so that the sum of the teal, purple and grey lines at a specific lead and Z500 averaging window is 100%. Lighter (darker) colors denote shorter (longer) temporal Z500 averaging windows.

Overall, we find that the ENSO-network alone (teal) contributes more frequently to correct predictions than the MJO-network alone (purple) for almost all leads and Z500 averaging windows. At shorter Z500 averaging windows (2 and 7 days), the MJO-network contributes more frequently until about a lead of 14-18 days, after which the ENSO-network becomes more frequently correct regardless of Z500 averaging windows. The most fre-

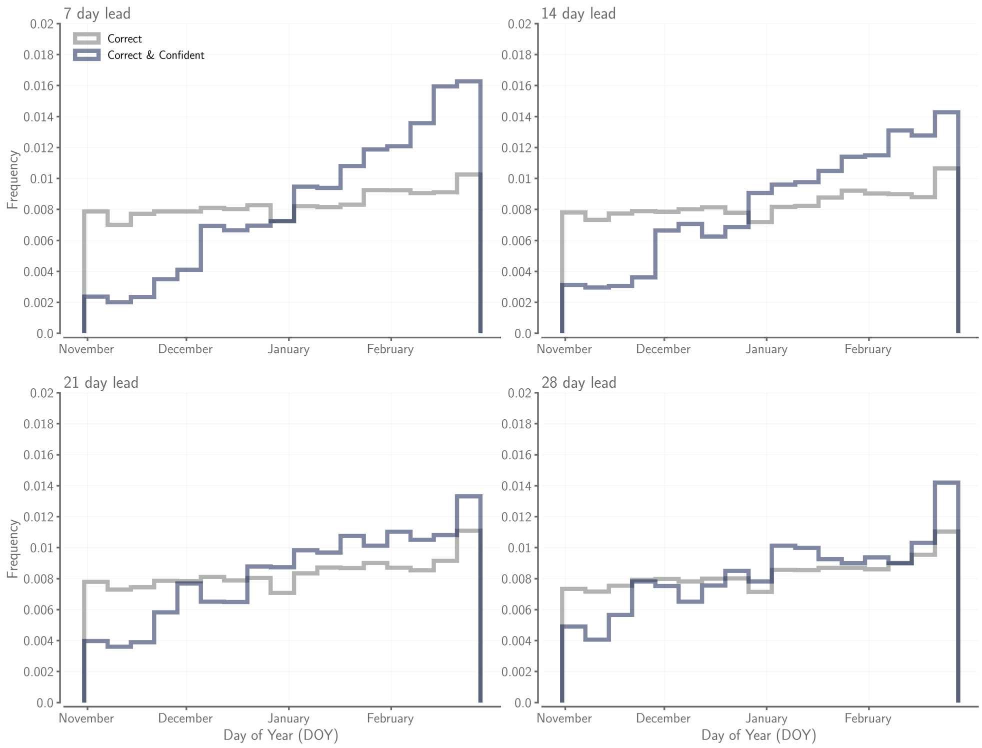


**Figure 2.** Frequency of a correct (grey) and confident (purple) network predictions by day of year (DOY) for a lead of 7, 14, 21, and 28 days across all Z500 averaging windows.

quently correct network combination is when *both* networks agree on the correct prediction (grey lines). However, the information provided by the ENSO state begins to contribute as frequently at leads greater than 21 days and longer averaging windows (darker teal lines). In general, as either the Z500 averaging window or lead time increases, the ENSO-network alone contributes more frequently to a correct prediction than the MJO-network. These results show that while the MJO-state is important for making predictions, ENSO plays a greater role in making correct subseasonal predictions for the majority of lead times and Z500 averaging windows.

If we further subset the predictions into correct and confident predictions (i.e. network-identified forecasts of opportunity), a similar though more exaggerated, story emerges. After a lead of 7 days, the ENSO-network contributes more frequently to correct and confident predictions than the MJO-network, regardless of Z500 averaging window (Figure 3b). At shorter leads the most frequent correct, confident predictions still occur when *both* the ENSO- and MJO-network correctly contribute to the predictions. However, the ENSO-network alone rivals these frequencies after a lead of 21 days. These results again demonstrate that the ENSO-network alone is generally more useful for correct (and confident) subseasonal predictions than the MJO-network.

When confident and correct predictions are further separated into positive and negative Z500 anomaly predictions, the contributions become more nuanced (Fig. 3b.1- b.2). For negative predictions, the ENSO-network more frequently contributes to correct, confident predictions than the MJO-network, regardless of lead time or averaging window. However, when examining positive predictions [note change to y-axis limits], the MJO-network alone contributes to correct, confident predictions more frequently than the ENSO-network at 5-7 day leads and Z500 averaging windows of 2 and 7 days (Fig. 3b.2). This

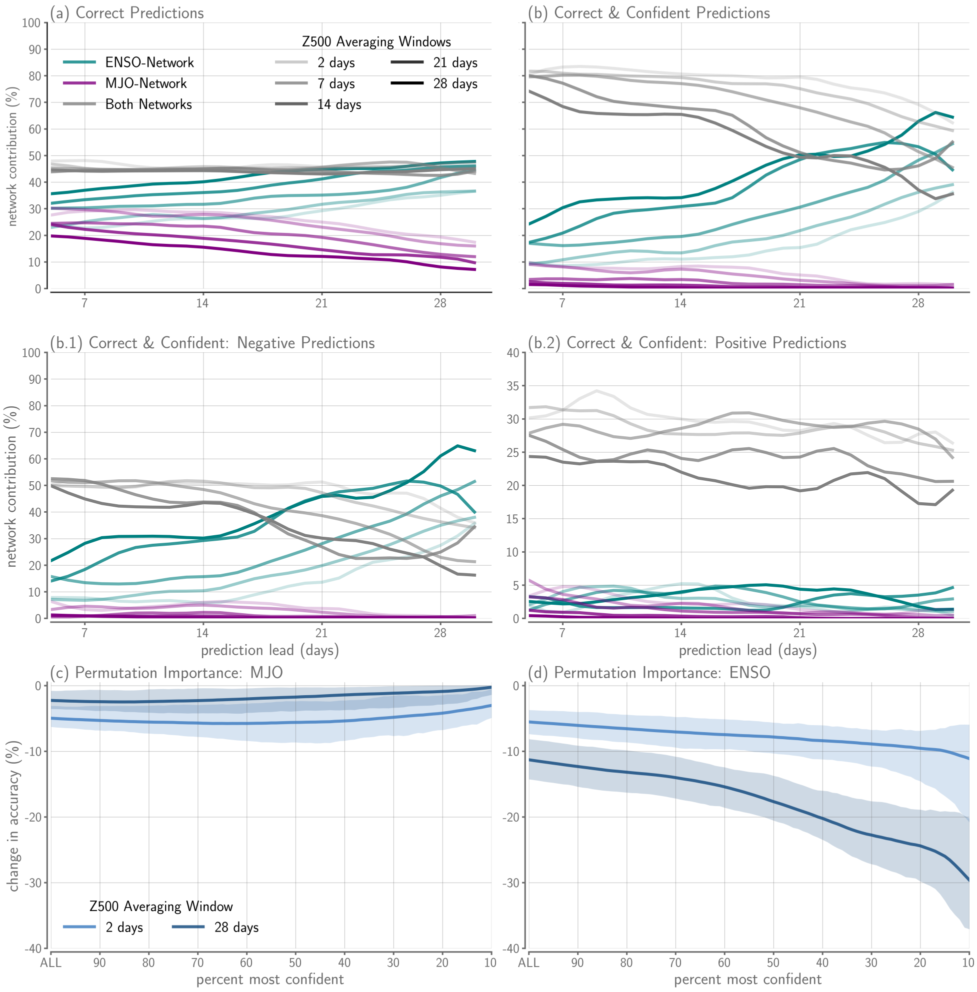


**Figure 3.** The frequency of a correct prediction provided by *either* the MJO- (purple) or ENSO-network (teal) or by *both* MJO- and ENSO-networks (grey) for each prediction lead. Lighter (darker) lines indicate shorter (longer) Z500 averaging windows. (b) As in (a) but for correct and confident predictions, which is further divided into (b.1) positive and (b.2) negative Z500 predictions [note different y-axis limits]. Lines are smoothed with a 3 day triangle filter for ease of interpretation. (c,d) Change in accuracy across confidence thresholds after permuting (c) RMM and (d) ENSO index input. The light/dark blue lines represent the mean of a 2 day/28 day Z500 averaging window across all lead times and the associated range of change in accuracy is represented by the shading.

suggests the MJO state is especially important for subseasonal prediction of anomalously high Z500 at shorter leads and averaging windows, particularly when the ENSO state is not useful (e.g. ENSO neutral conditions).

The utility of the MJO-network to the total network can be further elucidated when the prediction problem is, for example, constructed with a lead of 10 days and a Z500 averaging window of 5 days. We find that 42% of correct, confident positive Z500 anomaly predictions are periods with ENSO neutral conditions, when the tropical ocean should have the least control on the extratropical eastern Pacific. This is in stark contrast to confident, correct negative predictions which only occur in ENSO neutral states in 12% of cases. With that said, we note that negative predictions, of which the ENSO-network dominates, are overall more frequently confident and correct than positive predictions (Fig. 3b.1).

The results of the relative network contributions generally suggests the ENSO-network is the main contributor to correct (and confident) predictions. However, the MJO-network shows its utility for positive predictions when the network is correct and confident. We can further explore the impact of the MJO-network and ENSO-network on prediction skill through permutation importance (Figure 3c,d). In particular, we can quantify the contribution of the ENSO-network to the accuracy of the total network (Figure 3d) by randomly shuffling the input into the ENSO-network. In doing so, we separate the connection between the predictor and predictand, and thus, the predictors importance for making correct predictions. We find that across lead (shading) and Z500 averaging window (lines), the ENSO-network contributes between 5-12% for all predictions and close to 40% when the network is very confident. When permutation importance is instead applied to the MJO-network (Figure 3c), this contribution is about 1-5% across confident thresholds. We again only include the two extreme Z500 averaging windows for visualization, however, the other averaging window results lie within these curves. This further demonstrates that information provided by the ENSO-network is more important for higher skill, particularly at high confidence values (i.e. during forecasts of opportunity), compared to the MJO-network.

#### *3.2.1 MJO-Network Importance*

In general, our network indicates that ENSO is a more consistent provider of forecast skill of Z500 anomalies over the North Pacific. Nevertheless, there are specific time frames when the MJO-network provides important information for predicting Z500. To delve deeper into the MJO's optimal state for subseasonal predictability of Z500 in the North Pacific, K-means clustering is employed on the input features of the MJO network (RMM1 and RMM2). For brevity, we focus on a single lead time and averaging window (10 days and 5 days, respectively). This was found as a lead time and averaging window of relative peak importance for MJO driven predictability (Fig. 3b). This analysis focuses on instances when the network is confident and accurate, only during neutral ENSO conditions. We employ elbow and silhouette analysis to ascertain the optimal number of clusters for both positive and negative confident and correct predictions (Fig. S2, Rousseeuw, 1987). These methods offer a quantitative measure of how well-defined and separated the clusters are, providing insights into the cohesion within each cluster and the distinctiveness between clusters. This ensures a more nuanced evaluation of the clustering structure and reinforces our confidence in the appropriateness of the chosen number of clusters (3; Figure S2). The silhouette analysis shows clearly separated clusters which enhances the reliability of our clustering results, contributing to the overall robustness of our analysis. We then take a mean across the temporal dimension of each cluster to form a cluster composite of the input MJO RMM1/RMM2 predictor variables. Composites of the three clusters, for positive (top row) and negative (bottom row) Z500 anomaly predictions, are shown in figure 4.

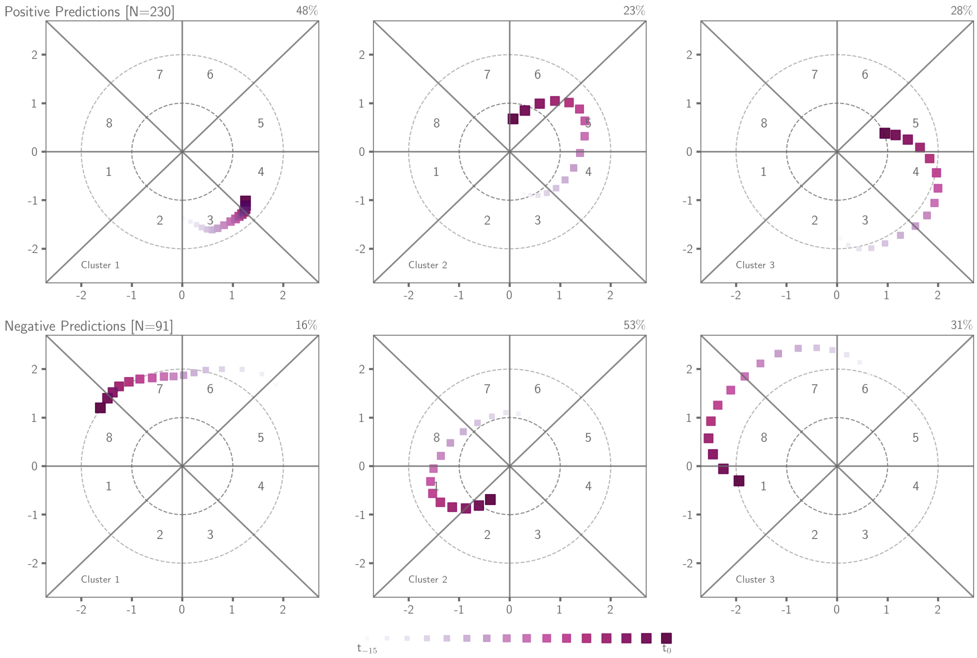


**Figure 4.** Composite clusters of MJO events when predictions are confident, correct, and ENSO is in a neutral state for anomalously high (top row) and anomalously low (bottom row) Aleutian Low states. Forecast lead is 10 days and a Z500 averaging window of 5 days. The RMM indices progress in time from light- $[t_{-15}]$ to dark- $[t_0]$ colors.

Firstly, we observe the frequency of events in which ENSO is neutral and the network exhibits both confident and correct predictions, represented as an N value in each row. Positive predictions are approximately 2.5 times more likely than negative events to exhibit this forecast condition (N=230 vs. N=91). This implies that the network demonstrates greater confidence and accuracy when forecasting positive Z500 anomalies during ENSO neutral states. Consequently, the MJO proves to be a more effective predictor (in CESM2-PI) in phases 3/4, where downstream Rossby wave dispersion leads to positive Z500 North Pacific anomalies. It is important to note that this does not necessarily imply that positive anomalies are universally more predictable at the subseasonal range, as the total number of confident, correct negative predictions is higher than those predicting a positive state (refer to the discussion of Fig. 3 for further details), and this is largely driven by ENSO positive events.

Positive predictions (row 1; high Z500 anomalies) show three distinct developing MJO states. Each developing MJO state is consistent with the phases that lead to a downstream positive Z500 anomaly (peaking in phases 3/4/5), demonstrating that the neural network has identified a physically justifiable link between the MJO and North Pacific circulation. Every cluster is above the threshold for active MJO events (1 sigma, inner dashed circle), and cluster 3 has periods which are above the 2 standard deviation threshold (97.5 percentile; outer dashed circle). Meaning, extremely anomalous events more consistently produce downstream extra-tropical Z500 anomalies. Cluster 1 shows a persistent anomaly in which the MJO stalls in between phases 3 and 4. These persistent cases have been previously identified as exciting a greater teleconnection response than fast moving MJO events (Yadav & Straus, 2017; Yadav et al., 2024). Finally, clusters 2 and 3 show events that are anomalously strong which then decay into MJO neutral states as they move towards initialization time. This is logical as MJO phase 6/7/8 is associated with a negative Z500 anomaly and thus would negate the current Z500 positive prediction at subseasonal forecast leads. To the author's knowledge, this is a unique aspect of this analysis showing that selective extremely anomalous MJO phases which then decay to a neutral MJO state can lead to enhanced subseasonal forecast skill, by *not* sparking MJO induced Rossby wave destructive interference. For the sake of brevity, we will simply note that the negative Z500 predictions (row2; low Z500 anomalies), largely mirror the findings found in the positive Z500 predictions.

The authors acknowledge that the MJO and ENSO indices along with the day of year are the sole information available to the network for making predictions. Keeping this limitation in mind, in summary, the subseasonal predictability of the Eastern North Pacific Z500 anomaly is predominantly influenced by highly active or persistent MJO events during neutral ENSO conditions. Larger anomalies result in increased predictability, and MJO events with substantial anomalies that subsequently transition into neutral states significantly contribute to subseasonal forecast skill.

## 4 Conclusion

This study aims to use an interpretable neural network to enhance the scientific understanding of the contribution of two tropical modes of variability to subseasonal predictability over the North Pacific: the MJO and ENSO. We find the network performs well on both the CESM2-PI testing data and ERA5 reanalysis across the range of lead time and averaging windows evaluated, suggesting the network is able to identify physically relevant sources of predictability. Further, the network is able to identify a late boreal winter preference for enhanced subseasonal predictability (Fig. 2), consistent with previous research which explores the importance of the subseasonal evolution of the background state for teleconnection propagation (e.g., Kumar & Hoerling, 1998; Chapman et al., 2021). This area of predictability research remains relatively unexplored, calling for more focused investigation.

Through an analysis of the relative roles of the MJO- and ENSO-networks, we find that forecast lead time and predictand averaging windows have a limited effect on the relative importance of MJO-driven North Pacific variability. ENSO dominates as the primary driver of subseasonal predictability for the majority of lead times and averaging windows, particularly at forecast ranges exceeding 7 days and averaging windows greater than 2 days (Fig. 3b,d). However, the MJO does provide some utility for prediction of positive Z500 anomalies during ENSO neutral states. In particular, persistent and particularly anomalous MJO events that decay before creating destructive interference offer the greatest utility for subseasonal predictability from the MJO in this region (Fig. 4).

The authors acknowledge that we predict the *sign* of the Aleutian Low anomaly and the relative importance of each predictor variable could change if the predictive target is changed to forecasting the magnitude or other, downstream affects of the MJO or ENSO (i.e., two-meter temperature or precipitation). Further, these results are for the CESM2-PI simulation, and therefore, does not account for possible affects from anthropogenic climate change. Recent research has shown that the MJO has become and will likely continue to become more predictable in a future climate (Du et al., 2023), which could subsequently improve midlatitude subseasonal skill provided by the MJO. On the other hand, previous research suggests ENSO may be the main tropical driver of future midlatitude subseasonal predictability changes (Mayer & Barnes, 2022). Therefore, future research should explore how our results may change in a future, warmer climate.

Given the chaotic nature of the weather system, a priori identification of particularly predictive windows offers a useful way forward for long range forecast skill (Albers & Newman, 2019; Mariotti et al., 2020). Ultimately, this paper demonstrates that interpretable neural networks can be used to gain physical insight into predictability, particularly through dissecting the relative importance of modes of variability thought important for subseasonal predictability.

## 5 Open Research

To promote transparency and reproducibility, all model training scripts and figures are readily accessible and can be downloaded using the provided code available on GitHub (https://github.com/kjmayer/ENSOvsMJO ; Mayer & Chapman, 2024). Comprehensive instructions for each step of this study are documented in the repository's README file. The authors leveraged the TensorFlow Python toolbox for machine learning and model training, a python machine learning environment can be found in this projects' repository. All data was produced as a part of the Community Earth System Model's contribution to the CMIP6 suite and is archived at the U.S. National Science Foundation's National Center for Atmospheric Research (NSF NCAR) computational and information systems lab (https://www2.cisl.ucar.edu/computing-data/data/cmip6-data-sets-glade). Raw ERA5 Reanalysis data can be obtained on the NSF NCAR Research Data Archive at: https://rda.ucar.edu/datasets/ds633.0/. Intermediate data files that can be leveraged to run every neural network and produce every plot specified in the github repo are stored at NCAR's Geoscience Data Exchange (Chapman & Mayer, 2024).

**Acknowledgments**

The work conducted by KJM is supported by the U.S. Department of Energy, Office of Science, Office of Biological & Environmental Research (BER), Regional and Global Model Analysis (RGMA) component of the Earth and Environmental System Modeling Program under Award Number DE-SC0022070 and National Science Foundation (NSF) IA 1947282. WEC received M²LInES research funding by the generosity of Eric and Wendy Schmidt by recommendation of the Schmidt Futures program. Further, this material is based upon work supported by the U.S. National Science Foundation under Grant No. AGS - 2230301 (NSF SOARS). Additionally, this work was supported by the U.S. National Science Foundation National Center for Atmospheric Research (NSF NCAR), which is a major facility sponsored by the NSF under Cooperative Agreement No. 1852977. Any opinions, findings, and conclusions or recommendations expressed in this material are those of the author(s) and do not necessarily reflect the views of the U.S. National Science Foundation.

We thank Dr. Emily Gordon for her insight and advice on using this interpretable neural networks.

## References

Agarwal, R., Melnick, L., Frosst, N., Zhang, X., Lengerich, B., Caruana, R., & Hinton, G. (2020, April). Neural additive models: Interpretable machine learning with neural nets.

Albers, J. R., & Newman, M. (2019). A priori identification of skillful extratropical subseasonal forecasts. *Geophysical Research Letters*, *46*(21), 12527–12536.

Arcodia, M. C., Kirtman, B. P., & Siqueira, L. S. P. (2020). How MJO teleconnections and ENSO interference impacts US precipitation. *J. Clim.*.

Capotondi, A., Deser, C., Phillips, A., Okumura, Y., & Larson, S. (2020). Enso and pacific decadal variability in the community earth system model version 2. *Journal of Advances in Modeling Earth Systems*, *12*(12), e2019MS002022.

Chapman, W. E., & Mayer, K. J. (2024). *Data for Exploring the Relative Contribution of the MJO and ENSO to Midlatitude Subseasonal Predictability [Dataset].* doi: https://doi.org/10.5065/f21v-ya03

Chapman, W. E., Subramanian, A. C., Xie, S.-P., Sierks, M. D., Ralph, F. M., & Kamae, Y. (2021). Monthly modulations of enso teleconnections: Implications for potential predictability in north america. *Journal of Climate*, *34*(14), 5899–5921.
Danabasoglu, G., Lamarque, J.-F., Bacmeister, J., Bailey, D., DuVivier, A., Edwards, J., ... others (2020). The community earth system model version 2 (cesm2). *Journal of Advances in Modeling Earth Systems*, *12*(2), e2019MS001916.
Davenport, F. V., & Diffenbaugh, N. S. (2021, July). Using machine learning to analyze physical causes of climate change: A case study of U.S. midwest extreme precipitation. *Geophys. Res. Lett.*.
Du, D., Subramanian, A. C., Han, W., Chapman, W. E., Weiss, J. B., & Bradley, E. (2023). Increase in mjo predictability under global warming. *Nature Climate Change*, 1–7.
Feldstein, S. B. (2002). Fundamental mechanisms of the growth and decay of the pna teleconnection pattern. *Quarterly Journal of the Royal Meteorological Society: A journal of the atmospheric sciences, applied meteorology and physical oceanography*, *128*(581), 775–796.
Frederiksen, J. (1983). A unified three-dimensional instability theory of the onset of blocking and cyclogenesis. ii. teleconnection patterns. *Journal of Atmospheric Sciences*, *40*(11), 2593–2609.
Gibson, P. B., Chapman, W. E., Altinok, A., Delle Monache, L., DeFlorio, M. J., & Waliser, D. E. (2021). Training machine learning models on climate model output yields skillful interpretable seasonal precipitation forecasts. *Communications Earth & Environment*, *2*(1), 159.
Gordon, E. M., Barnes, E. A., & Davenport, F. V. (2023). Separating internal and forced contributions to near term sst predictability in the cesm2-le. *Environmental Research Letters*.
Gordon, E. M., Barnes, E. A., & Hurrell, J. W. (2021, November). Oceanic harbingers of pacific decadal oscillation predictability in CESM2 detected by neural networks. *Geophys. Res. Lett.*, *48*(21).
Henderson, S. A., & Maloney, E. D. (2018, July). The impact of the Madden–Julian oscillation on High-Latitude winter blocking during el niño–southern oscillation events. *J. Clim.*, *31*(13), 5293–5318.
Henderson, S. A., Maloney, E. D., & Barnes, E. A. (2016). The influence of the madden–julian oscillation on northern hemisphere winter blocking. *Journal of Climate*, *29*(12), 4597–4616.
Hendon, H. H., Zhang, C., & Glick, J. D. (1999, August). Interannual variation of the Madden–Julian oscillation during austral summer. *J. Clim.*, *12*(8), 2538–2550.
Hersbach, H., Bell, B., Berrisford, P., Hirahara, S., Horányi, A., Muñoz-Sabater, J., ... others (2020). The era5 global reanalysis. *Quarterly Journal of the Royal Meteorological Society*, *146*(730), 1999–2049.
Hoskins, B. J., & Ambrizzi, T. (1993, June). Rossby wave propagation on a realistic longitudinally varying flow. *J. Atmos. Sci.*, *50*(12), 1661–1671.
Johnson, N. C., Collins, D. C., Feldstein, S. B., L'Heureux, M. L., & Riddle, E. E. (2014, February). Skillful wintertime north american temperature forecasts out to 4 weeks based on the state of ENSO and the MJO. *Weather Forecast.*, *29*(1), 23–38.
Johnson, N. C., Collins, D. C., Feldstein, S. B., L'Heureux, M. L., & Riddle, E. E. (2014). Skillful wintertime north american temperature forecasts out to 4 weeks based on the state of enso and the mjo. *Weather and Forecasting*, *29*(1), 23–38.
Kessler, W. S. (2001, July). EOF representations of the Madden–Julian oscillation and its connection with ENSO. *J. Clim.*, *14*(13), 3055–3061.
Kingma, D. P., & Ba, J. (2014). Adam: A method for stochastic optimization. *arXiv preprint arXiv:1412.6980*.

Kumar, A., & Hoerling, M. P. (1998). Annual cycle of pacific–north american seasonal predictability associated with different phases of enso. *Journal of Climate*, *11*(12), 3295–3308.

Labe, Z. M., & Barnes, E. A. (2022, May). Predicting slowdowns in decadal climate warming trends with explainable neural networks. *Geophys. Res. Lett.*.

Lin, H., Brunet, G., & Derome, J. (2008). Forecast skill of the madden–julian oscillation in two canadian atmospheric models. *Monthly Weather Review*, *136*(11), 4130–4149.

Madden, R. A., & Julian, P. R. (1971, July). Detection of a 40–50 day oscillation in the zonal wind in the tropical pacific. *J. Atmos. Sci.*, *28*(5), 702–708.

Madden, R. A., & Julian, P. R. (1972, September). Description of Global-Scale circulation cells in the tropics with a 40–50 day period. *J. Atmos. Sci.*, *29*(6), 1109–1123.

Madden, R. A., & Julian, P. R. (1994, May). Observations of the 40–50-day tropical Oscillation—A review. *Mon. Weather Rev.*, *122*(5), 814–837.

Mariotti, A., Baggett, C., Barnes, E. A., Becker, E., Butler, A., Collins, D. C., ... Albers, J. (2020, January). Windows of opportunity for skillful forecasts subseasonal to seasonal and beyond. *Bull. Am. Meteorol. Soc.*.

Martin, Z. K., Barnes, E. A., & Maloney, E. (2022, May). Using simple, explainable neural networks to predict the Madden-Julian oscillation. *J. Adv. Model. Earth Syst.*.

Mayer, K. J., & Barnes, E. A. (2021, May). Subseasonal forecasts of opportunity identified by an explainable neural network. *Geophys. Res. Lett.*.

Mayer, K. J., & Barnes, E. A. (2022, July). Quantifying the effect of climate change on midlatitude subseasonal prediction skill provided by the tropics. *Geophys. Res. Lett.*, *49*(14).

Mayer, K. J., & Chapman, W. E. (2024). *Code (Version 1.0.0) for Exploring the Relative Contribution of the MJO and ENSO to Midlatitude Subseasonal Predictability [Software]. Zenodo.* Retrieved from `https://github.com/kjmayer/ENSOvsMJO` doi: https://doi.org/10.5281/zenodo.10607685

McGovern, A., Lagerquist, R., Gagne, D. J., Jergensen, G. E., Elmore, K. L., Homeyer, C. R., & Smith, T. (2019). Making the black box more transparent: Understanding the physical implications of machine learning. *Bulletin of the American Meteorological Society*, *100*(11), 2175–2199.

Merryfield, W. J., Baehr, J., Batté, L., & others. (2020). Current and emerging developments in subseasonal to decadal prediction. *Bulletin of the*.

Moon, J.-Y., Wang, B., & Ha, K.-J. (2011, September). ENSO regulation of MJO teleconnection. *Clim. Dyn.*, *37*(5), 1133–1149.

Namias, J. (1986, July). Persistence of flow patterns over north america and adjacent ocean sectors. *Mon. Weather Rev.*, *114*(7), 1368–1383.

Newman, M., & Sardeshmukh, P. D. (1998). The impact of the annual cycle on the north pacific/north american response to remote low-frequency forcing. *Journal of the Atmospheric Sciences*, *55*(8), 1336–1353.

Philander, S. (1985). El niño and la niña. *Journal of Atmospheric Sciences*, *42*(23), 2652–2662.

Pohl, B., & Matthews, A. J. (2007, June). Observed changes in the lifetime and amplitude of the Madden–Julian oscillation associated with interannual ENSO sea surface temperature anomalies. *J. Clim.*, *20*(11), 2659–2674.

Rousseeuw, P. J. (1987). Silhouettes: a graphical aid to the interpretation and validation of cluster analysis. *Journal of computational and applied mathematics*, *20*, 53–65.

Sardeshmukh, P. D., & Hoskins, B. J. (1988). The generation of global rotational flow by steady idealized tropical divergence. *Journal of the Atmospheric Sciences*, *45*(7), 1228–1251.

Simmons, A., Wallace, J., & Branstator, G. (1983). Barotropic wave propagation and instability, and atmospheric teleconnection patterns. *Journal of the Atmospheric Sciences*, *40*(6), 1363–1392.

Stan, C., Straus, D. M., Frederiksen, J. S., Lin, H., Maloney, E. D., & Schumacher, C. (2017, December). Review of Tropical-Extratropical teleconnections on intraseasonal time scales: The subseasonal to seasonal (S2S) teleconnection Sub-Project. *Rev. Geophys.*, *55*(4), 902–937.

Takahashi, C., & Shirooka, R. (2014, September). Storm track activity over the north pacific associated with the Madden-Julian oscillation under ENSO conditions during boreal winter. *J. Geophys. Res.*, *119*(18), 10,663–10,683.

Toms, B. A., Barnes, E. A., & Ebert-Uphoff, I. (2020, September). Physically interpretable neural networks for the geosciences: Applications to earth system variability. *J. Adv. Model. Earth Syst.*, *12*(9).

Toms, B. A., Kashinath, K., Yang, D., & Prabhat. (2021, July). Testing the reliability of interpretable neural networks in geoscience using the Madden–Julian oscillation. *Geosci. Model Dev.*, *14*(7), 4495–4508.

Trenberth, K. E. (1997). The definition of el nino. *Bull. Am. Meteorol. Soc.*, *78*(12), 2771–2778.

Tseng, K.-C., Barnes, E. A., & Maloney, E. D. (2018, January). Prediction of the midlatitude response to strong Madden-Julian oscillation events on S2S time scales: PREDICTION OF Z500 AT S2S TIME SCALES. *Geophys. Res. Lett.*, *45*(1), 463–470.

Tseng, K.-C., Maloney, E., & Barnes, E. A. (2020, May). The consistency of MJO teleconnection patterns on interannual time scales. *J. Clim.*, *33*(9), 3471–3486.

Vitart, F., Ardilouze, C., Bonet, A., Brookshaw, A., Chen, M., Codorean, C., ... Zhang, L. (2017, January). The subseasonal to seasonal (S2S) prediction project database. *Bull. Am. Meteorol. Soc.*, *98*(1), 163–173.

Vitart, F., Robertson, A. W., & Anderson, D. L. T. (2012, January). Subseasonal to seasonal prediction project: Bridging the gap between weather and climate. *WMO Bull.*, *61*(61).

Wallace, J. M., & Gutzler, D. S. (1981). Teleconnections in the geopotential height field during the northern hemisphere winter. *Monthly weather review*, *109*(4), 784–812.

Wang, J., Kim, H., & DeFlorio, M. J. (2022). Future changes of pna-like mjo teleconnections in cmip6 models: Underlying mechanisms and uncertainty. *Journal of Climate*, *35*(11), 3459–3478.

Wang, L., & Robertson, A. W. (2019, May). Week 3–4 predictability over the united states assessed from two operational ensemble prediction systems. *Clim. Dyn.*, *52*(9), 5861–5875.

Wheeler, M. C., & Hendon, H. H. (2004). An all-season real-time multivariate mjo index: Development of an index for monitoring and prediction. *Monthly weather review*, *132*(8), 1917–1932.

White, C. J., Carlsen, H., Robertson, A. W., Klein, R. J. T., Lazo, J. K., Kumar, A., ... Zebiak, S. E. (2017, July). Potential applications of subseasonal-to-seasonal (S2S) predictions. *Met. Apps*, *24*(3), 315–325.

White, C. J., Domeisen, D. I. V., Acharya, N., Adefisan, E. A., Anderson, M. L., Aura, S., ... Wilson, R. G. (2021, November). Advances in the application and utility of subseasonal-to-seasonal predictions. *Bull. Am. Meteorol. Soc.*, *-1*(aop), 1–57.

Winkler, C. R., Newman, M., & Sardeshmukh, P. D. (2001). A linear model of wintertime low-frequency variability. part i: Formulation and forecast skill. *Journal of climate*, *14*(24), 4474–4494.

Yadav, P., Garfinkel, C. I., & Domeisen, D. I. (2024). The role of the stratosphere in teleconnections arising from fast and slow mjo episodes. *Geophysical Research Let-*

*ters*, *51*(1), e2023GL104826.

Yadav, P., & Straus, D. M. (2017). Circulation response to fast and slow mjo episodes. *Monthly Weather Review*, *145*(5), 1577–1596.

Zhuang, J., Dussin, R., Jüling, A., & Rasp, S. (2018). xesmf: Universal regridder for geospatial data. *Zenodo [code]*, *10*.

# Supporting Information for "Exploring the Relative Contribution of the MJO and ENSO to Midlatitude Subseasonal Predictability"

Kirsten J. Mayer[1*], William E. Chapman[1*], William A. Manriquez[2]

[1]U.S. National Science Foundation National Center for Atmospheric Research

[2]Metropolitan State University of Denver

*These authors contributed equally

## Contents of this file



## Introduction

In this supplemental material, we present two figures of which support the main analysis: CESM2-PI representation of MJO teleconnections and optimal clustering selection.

**Text S1.** Figure S1 shows the frequency of a positive Z500 anomaly 5-9 days following an active MJO event in phase 6/7 (Column I) or phase 3/4 (Column II) in the ERA5 (row I) and the CESM2-PI (row II) during extended boreal winter (November-March). Blue/red shading indicates that a negative/positive anomaly is more frequent 5-9 days following the MJO event. We see that CESM2-PI has a relatively good representation of the MJO teleconnection, motivating the utility of CESM2-PI for our analysis.

**Text S2.** Figure S2 shows the silhouette analysis (top) and elbow method (bottom) to identify the optimal number ('K') clusters for K-means clustering, particularly for samples when the network is confident and accurate during neutral ENSO conditions. Three clusters are selected for our analysis as the is where the silhouette score is maximized and the elbow method is minimized.

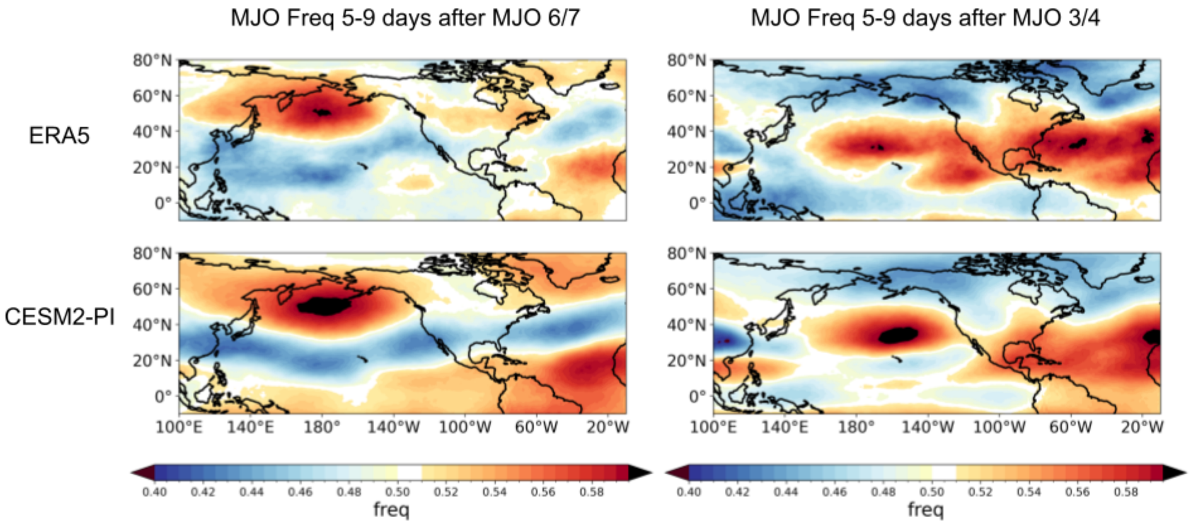


**Figure S1.** Frequency of a positive Z500 anomaly 5-9 days after an active MJO event in phase 6/7 (Column I) or phase 3/4 (Column II) in the ERA5 (row I) and the CESM2-PI (row II) in NDJFM. Composites span model years 100-400 for the CESM2-PI and 1979-2020 for the ERA5

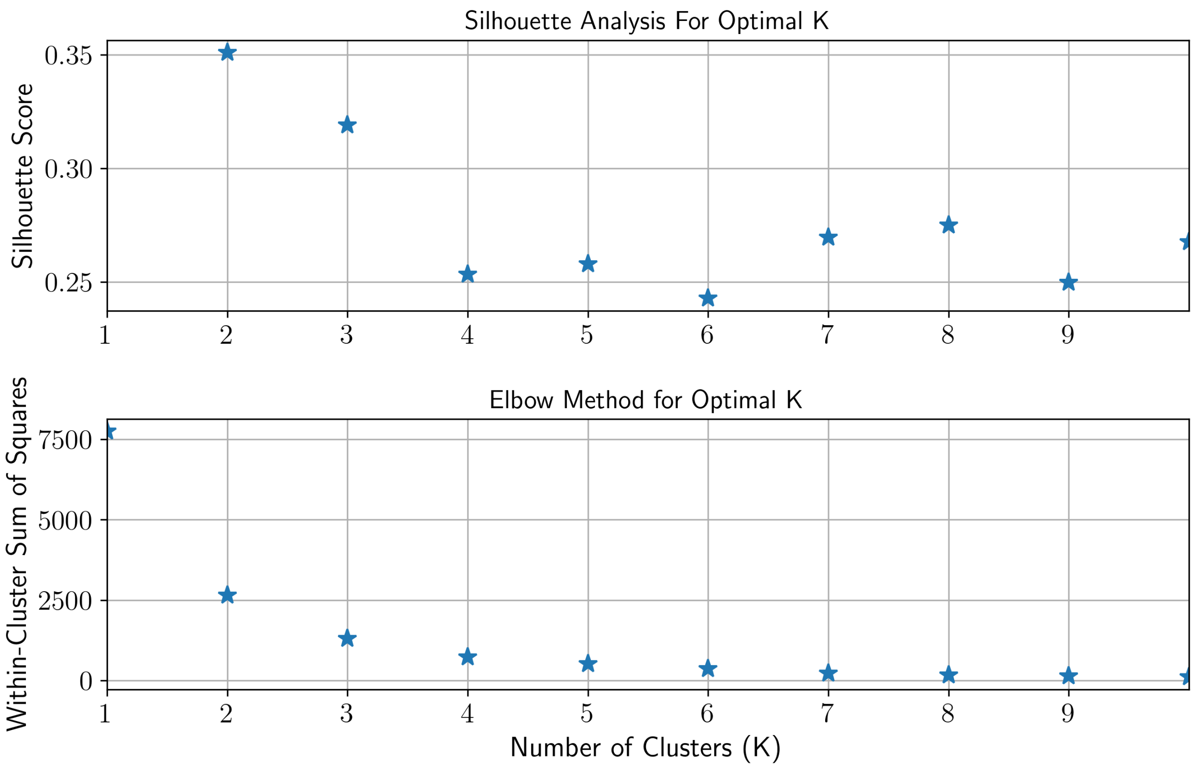


**Figure S2.** Silhouette analysis and elbow method for optimal selection of K clusters